t-AUCB, a Pharmacological Inhibitor of Soluble Epoxide Hydrolase, Promotes Brown Adipogenesis: Role of PPAR alpha and PPAR gamma

A Thesis Presented for the
Master of Science
Degree
The University of Tennessee, Knoxville

Kelsey Jo Hildreth
December 2019

ACKNOWLEDGMENTS

I would like to thank my advisor, Dr. Ling Zhao, and my committee members, Dr. Bettaieb and Dr. Chen, for their guidance throughout my graduate studies. I would also like to thank my classmates and lab partners, Haley Overby, Emily Hager, Katie Graham, Yang Yang, and Bohye Park for helping me throughout my coursework and research.

ABSTRACT

Brown adipose tissue (BAT) has recently emerged as a novel target for obesity treatment and prevention. In contrast to the lipid storing function of white adipocytes, brown adipocytes are responsible for dissipating energy as heat, a process involving uncoupling protein 1 (UCP1). Soluble epoxide hydrolase (sEH) is a cytosolic enzyme that converts epoxy fatty acids (EpFAs) into less active diols. By stabilizing endogenous EpFAs, potent small molecule sEH inhibitors have been shown to be beneficial for many diseases. Several recent studies have reported that sEH inhibitors can improve diet-induced metabolic disorders, possibly by upregulating UCP1 expression. In the current study, we sought to investigate the mechanisms by which the sEH inhibition affects brown adipocytes using *trans*-4-[4-(3-adamantan-1-yl-ureido)-cyclohexyloxy]-benzoic acid (*t*-AUCB). The effects of *t*-AUCB on murine brown adipocyte differentiation were evaluated by lipid accumulation and expression of brown adipocyte marker genes. PPARα[alpha] and PPARγ[gamma] activation by *t*-AUCB was measured by their respective transactivation assays. The roles of PPARs were further studied by pharmacological antagonism and knockdown experiments. Finally, the mechanisms of *t*-AUCB were explored in BAT derived sEH wildtype (WT) and knockout (KO) stromal cells. We report that sEH expression was increased during murine brown adipocyte differentiation. *t*-AUCB dose-dependently promoted brown adipocyte differentiation. Moreover, we demonstrate that *t*-AUCB activated PPARα[alpha], but not PPARγ[gamma]. *t*-AUCB-induced upregulation of thermogenic genes *Ucp1, Pgc-1a,* and *Cidea* and the general differentiation marker *Fabp4* was significantly attenuated by the antagonist of PPARα[alpha], GW6471 and specific knockdown of *Pparα*. In contrast, upregulation was only partially attenuated by the antagonist of PPARγ[gamma],

GW9662, and specific knockdown of *Pparg*. We also show that *t*-AUCB activation of PPARα[alpha] occurs regardless of sEH presence. Our findings suggest that PPARα[alpha], more so than PPARγ[gamma], plays an important role in *t*-AUCB's effects on brown adipogenesis and that these effects may be independent of sEH.

TABLE OF CONTENTS

LIST OF FIGURES

ABBREVIATIONS

ATP-binding cassette transporter A1 (ABCA1), 5' adenosine monophosphate-activated protein kinase (AMPK), adipose tissue triglyceride lipase (ATGL), adenosine triphosphate (ATP), all-trans retinoic acid (ATRA), 12-(3-adamantan-1-yl-ureido) dodecanoic acid (AUDA), brown adipose tissue (BAT), beta-3 adrenergic receptor (β_3-AR), cyclic AMP (cAMP), CCAAT/enhancer-binding protein beta (C/EBP-β), cell death-inducing DFFA-like effector A (Cidea), N-cyclohexyl-N'-dodecanoic acid urea (CUDA), cytochrome P450 (CYP450), docosahexaenoic acid (DHA), dihydroxy fatty acids (DiHFAs), epoxyeicosatrienoic acids (EETs), eicosapentaenoic acid (EPA), epoxy fatty acids (EpFAs), extracellular signal–regulated kinase 1/2 (ERK 1/2), free fatty acids (FFA), fludeoxyglucose ($[^{18}F]$FDG), high carbohydrate, high fat (HCHF), high-fat diet (HFD), interscapular BAT (iBAT), (S)-2-(11-(nonyloxy)undec-8(Z)-enamido)succinic acid (NUDSA), positron emission tomography – computed tomography (PET/CT), PPARγ co-activator 1 alpha (PGC-1α), protein kinase A (PKA), peroxisome proliferator-activated receptor (PPAR), PRD1-F1-RIZ1 homologous domain containing 16 (PRDM16), polyunsaturated fatty acids (PUFA), retinoic acid (RA), retinoic acid receptor (RAR), retinoid X receptor (RXR), soluble epoxide hydrolase (sEH), soluble epoxide hydrolase inhibitor (sEHI), *trans*-4-[4-(3-adamantan-1-yl-ureido)-cyclohexyloxy]-benzoic acid (*t*-AUCB), transient receptor potential vanilloid type 1 (TRPV1), uncoupling protein 1 (UCP1), white adipose tissue (WAT)

CHAPTER I
INTRODUCTION

Obesity has become an epidemic, with more than 2.8 million people dying each year due to the comorbidities associated with being overweight or obese [1]. Obesity is characterized by the accumulation of excess white adipose tissue (WAT) which is a subclass of adipose tissue that stores energy as fat [2]. In contrast, brown adipose tissue (BAT) uses energy to produce heat [3]. It was previously thought that metabolically active BAT was only present in infants; however, studies have now found BAT to be present in small amounts in adult humans [2]. BAT is now being studied as a potential therapeutic target for the treatment of obesity and related metabolic diseases [3].

BAT prevalence has been negatively correlated with body mass index and body fat content [4, 5]. Additionally, BAT activation has been seen to improve insulin sensitivity, regulate glucose homeostasis, and accelerate triglyceride clearance [6, 7]. The possibility of enhancing energy-wasting and metabolic function through BAT activity has prompted extensive research. Several nutritional and pharmacological factors contributing to BAT development and activity by various mechanisms have been identified, but the search continues for safer and more effective options [8, 9].

Soluble epoxide hydrolase (sEH) is a cytosolic enzyme that converts epoxy fatty acids (EpFAs) to diols, typically reducing their biological activity [10, 11]. sEH expression has been found to be positively correlated with body weight in mouse and human adipose tissue [12]. sEH inhibitors (sEHIs) have been shown to be beneficial for many disease states [13]. The inhibition or knockout of sEH in cell and animal studies have proven effective in ameliorating obesity-

related metabolic disorders [14]. While the potential for sEH inhibition to promote weight loss and directly combat obesity is unclear, it has been shown to activate BAT and prevent weight gain in a high-fat diet mouse model [15, 16]. Many different sEHIs have been developed and found to be effective in various species and physiologies [17]. *t*-AUCB (*trans*-4-[4-(3-adamantan-1-yl-ureido)-cyclohexyloxy]-benzoic acid) is an especially promising sEHI with superior solubility and stability as well as high bioavailability and potency across species [18]. sEHIs have entered human trials have and have, so far, been determined to be safe [19, 20]. The exact mechanisms of the sEHIs are largely unknown. In most studies, sEHI effects have been attributed to the stabilization of endogenous EpFAs, particularly EETs (epoxyeicosatrienoic acids) [11, 13, 21]. sEHIs were designed to mimic EETs [22], which are known peroxisome proliferator-activated receptor alpha (PPARα) [23], and gamma (PPARγ) [24] ligands. Two sEHIs, CUDA (N-cyclohexyl-N'-dodecanoic acid urea) and AUDA, have been found to directly activate PPARα, but not PPARδ or PPARγ [25]. The PPARs are especially significant to our research because of their role in adipogenesis. The objective of this thesis is to study the mechanisms by which the sEH inhibitor *t*-AUCB acts on brown preadipocytes, specifically the role of PPARα and PPARγ. The results presented add to our understanding of *t*-AUCB and its therapeutic potential for obesity and related metabolic disease.

CHAPTER II
LITERATURE REVIEW

2.1 Brown Adipose Tissue: Function, Development, Metabolic Impact, and Regulation

2.1.1. Brown Adipose Tissue Function

Brown adipose tissue (BAT) is a thermoregulatory organ that is essential to non-shivering thermogenesis in response to cold exposure. In BAT, chemical energy can be converted to heat via uncoupling protein 1 (UCP1) present in the mitochondria, which are particularly abundant in BAT. UCP1 uncouples the electron transport chain from adenosine triphosphate (ATP) production, resulting in energy dissipation and heat production and thereby increased energy expenditure. UCP1-mediated thermogenesis relies on oxidative metabolism with lipids as the predominant energy source, but BAT also actively takes up glucose [3].

The development of BAT is thought to be crucial in the evolutionary success of mammals, as thermogenesis increases neonatal survival and allows mammals to adapt to cold environments [3]. BAT is found in specific locations in the body [3]. In rodents, BAT depots can be found in the interscapular, axillary, perirenal, and periaortic regions [3]. Human BAT has been identified in similar areas, with depots in the supraclavicular, cervical, and paraspinal regions [26]. BAT is only present in small amounts in adult mammals and to a lesser extent in obese individuals [27].

Although thermogenesis is the most studied function of BAT, recent findings reveal BAT involvement in triglyceride clearance, glucose disposal, secretion of signal molecules, and inflammation [7, 28-30]. For example, it was found that cold-induced BAT activity in mice decreases plasma triglyceride levels due to increased turnover of triglyceride-rich lipoproteins

and uptake of lipids into BAT through activation of CD36, a cell-surface fatty acid translocase [7]. BAT also serves as a major organ for glucose disposal in these mice, particularly the obese mice [7].

BAT also functions as a secretory organ, which may contribute to systemic consequences of BAT activity that are currently being explored [31] [28, 32]. Many regulatory molecules produced by BAT, called brown adipokines or batokines, have been identified such as fibroblast growth factor 21 (FGF21), interleukin 6 (IL-6), neuregulin 4 (NRG4), vascular endothelial growth factor A (VEGFA), and insulin-like growth factor 1 (IGF1) [28]. The systemic roles of batokines and the potential to take advantage of such molecules for pharmacological intervention are being researched extensively [33-35]

Additionally, BAT has been suggested to have an anti-inflammatory function [29, 30, 36]. During high-fat feeding in an obese state, immune cells and macrophages accumulate in WAT, triggering inflammation [29]. Under similar conditions, BAT does not appear to be infiltrated by macrophages, which may be due to the ability of BAT to quickly use free fatty acids and avoid lipotoxicity [29]. It was also found that macrophages in BAT do not share the same chemokine and cytokine expression as those in WAT, indicating that the microenvironment of BAT could be anti-inflammatory as opposed to the pro-inflammatory microenvironment of WAT [30, 36].

2.1.2. Brown Adipose Tissue Development

Brown adipocytes are derived from *Myf5*-expressing cells which are also the precursor for skeletal muscle cells and a subpopulation of white adipocytes [37, 38]. These cells develop to brown preadipocytes which then undergo differentiation to brown adipocytes [27]. BAT

development has been reported to be under the control of several transcriptional regulators, but peroxisome proliferator-activated receptor gamma (PPARγ) is the main transcription factor that is required under every circumstance for both white and brown adipocyte development [39]. PPARγ is a nuclear hormone receptor expressed mainly in white and brown adipose tissue [40]. Multiple levels of regulation of PPARγ allow for targeting of brown adipocyte-specific transcription [39]. Three PPAR isoforms that have highly conserved DNA-binding domains but more diverse ligand-binding domains have been identified as a subfamily of nuclear hormone receptors – PPARα, PPARβ/δ and PPARγ [40]. While PPARγ strongly induces adipogenesis and is the predominant PPAR isoform involved in this process, PPARα activation can also induce significant adipogenesis [40].

The association of PPARγ with other key regulators of brown adipogenesis, including PRD1-F1-RIZ1 homologous domain containing 16 (PRDM16) and PPARγ co-activator 1 alpha (PGC-1α), allows for selective regulation of adipogenic and thermogenic genes. PRDM16 has been shown to be responsible for controlling whether the *Myf5*-expressing progenitor cells become myocytes or brown adipocytes [41]. Overexpression of PRDM16 was found to convert myocytes into brown adipocytes [42]. Additionally, PRDM16 expression in adipose tissue induced thermogenic gene expression [42]. PRDM16 binds to other transcriptional regulators such as CCAAT/enhancer-binding protein beta (C/EBP-β), which induces PPARγ and PGC-1α expression in preadipocytes [41]. PRDM16 then binds PPARγ and PGC-1α and recruits the PPARγ transcription complex to the promoter regions of brown adipogenic and thermogenic genes [41].

PGC-1α is a cold-induced cofactor of PPARγ involved in thermogenic gene expression that is also a downstream target of the protein kinase A (PKA) – cyclic AMP – responsive element-binding protein 1 (CREB) signaling pathway and is post-transcriptionally controlled via phosphorylation [43]. PGC-1α interacts with PPARγ and directly induces UCP1 expression [44]. PGC-1α also acts as the primary regulator of multiple pathways related to mitochondrial biogenesis and thermogenesis [45].

2.1.3. Metabolic Impact of Brown Adipose Tissue

BAT is currently under investigation for its therapeutic potential in obesity and metabolic disease. In 1983, Rothwell and Stock predicted that in humans, stimulation of just a small amount of BAT, only 40 to 50 grams, could utilize up to 20% of an individual's daily energy expenditure [46]. Imaging studies in both mice and humans have shown that BAT mass is negatively correlated with body mass index and adiposity [4, 5]. In humans, there is some evidence of small amounts of fat mass loss due to increases in energy expenditure related to BAT [47]. However, studies of BAT activation in relation to weight loss in humans have overall been inconclusive [6, 48-50]. Inconsistencies in these studies can likely be attributed to variability in experimental protocols, type of intervention, measurement of BAT mass and activity, and human subjects.

In addition to its potential contribution to energy expenditure, BAT has been shown to have systemic impacts on processes such as glucose and lipid metabolism [6, 31, 51]. Free fatty acids (FFA) serve as the main substrate for BAT [3]. In rodents, BAT activation appears to enhance triglyceride clearance, reduce high cholesterol, and protect from atherosclerosis [7, 52]. In humans who underwent 5-8 hours of non-shivering cold exposure, BAT volume was found to

be significantly correlated with cold-induced increases in FFA oxidation, whole-body lipolysis, and triglyceride-FFA cycling as measured by stable isotope tracers and indirect calorimetry [31]. Cold exposure also led to increased plasma FFA and glycerol concentrations with no differences in plasma concentrations of triglycerides or cholesterol [31]. Fasting plasma concentrations of very-low-density lipoprotein (VLDL) cholesterol and triglycerides were decreased on the day after participants endured cold exposure [31]. These results suggest a possible metabolic benefit of stimulated BAT to induce lipid mobilization from adipose tissue to be used as BAT substrate for thermogenesis, as well as long-term benefits to lipid metabolism.

BAT also appears to have beneficial effects on glucose metabolism. BAT mass/activity has been seen to be lower in diabetic than non-diabetic individuals [53]. Using [^{18}F]FDG to trace glucose uptake and [^{15}O]H_2O to measure BAT respiration and determine perfusion rate, it was found that cold exposure (2 hours at 17°C ambient temperature followed by intermittent placement of one foot in 8°C water) induced a 12-fold increase in glucose uptake rate in human BAT accompanied by a doubling in BAT perfusion (indicative of thermogenesis) with no changes in glucose uptake rate in subcutaneous WAT, visceral adipose tissue, or skeletal muscle [51]. Another human study by Chondronikola et al. reported similar findings of cold exposure (5-8 hours at 19°C ambient temperature while wearing a Cool Flow vest and blanket that decreased from 20°C until the subject was shivering and was then maintained at 1°C above shivering) resulting in increased [^{18}F]FDG uptake in BAT but not in the liver, visceral adipose tissue, subcutaneous adipose tissue, or skeletal muscle [6].

Chondronikola et al. also determined, using PET/CT and indirect calorimetry, that the observed cold-induced glucose uptake in BAT significantly increased whole-body glucose

disposal [6]. The authors calculated that BAT, if able to remain chronically active, could dispose of about 23 grams of glucose per day [6]. Furthermore, the same cold-exposure conditions to induced BAT activation during hyperinsulinemia resulted in increases glucose disposal and insulin sensitivity as compared to hyperinsulinemic conditions in individuals without detectable BAT [6].

2.1.4 Regulators of Brown Adipose Tissue

One regulator of brown adipose tissue is cold exposure. Cold temperatures are sensed by certain transient receptor potential (TRP) channels expressed by nerve terminals [54]. These channels initiate signaling to the hypothalamus which then increases sympathetic signaling to BAT [55]. BAT is innervated by an abundance of nerve endings that release norepinephrine upon sympathetic stimulation [56]. The standard model of regulation of BAT thermogenesis begins with norepinephrine binding to β_3-adrenergic receptors (β_3-ARs) on the membrane of the brown adipocytes which causes activation of adenylyl cyclase and subsequent cyclic AMP (cAMP) production [57]. cAMP activates PKA which phosphorylates adipose tissue triglyceride lipase (ATGL) resulting in increased lipolysis within the adipocytes [57]. The released FFA then activate UCP1 [57]. However, this model has been questioned due to the observation that a lack of ATGL or the ATGL-activating protein CGI-58 within brown adipocytes in mice had no effect on non-shivering thermogenesis [58, 59]. Alternative models may be necessary to explain how β_3-AR agonists can activate UCP-1 without the intracellular release of FFA.

In addition to cold, an overwhelming number of very diverse factors have been proposed to regulate brown adipose tissue [9, 57]. Only a small selection of nutritional and pharmacological factors will be discussed here.

2.1.4.1 Capsaicin and Capsinoids

Some of the most studied nutritional regulators of BAT, capsaicin and capsinoids, are components found in certain peppers that have been shown to increase thermogenesis in mice and humans [60, 61]. In mice, treatment with a high-fat diet (HFD) containing capsinoids at a concentration of 0.3% (weight for weight) for 8 weeks with or without mild cold exposure (17 °C) resulted in significantly less body weight gain in the ambient temperature (25 °C) capsinoid-treated mice as compared to the ambient temperature vehicle-treated mice [60]. Furthermore, while cold exposure resulted in significantly less weight gain than ambient temperature regardless of capsinoid treatment, the cold-exposed, capsinoid-treated mice gained less weight than the cold-exposed vehicle-treated mice, indicating a synergistic effect of capsinoids and cold exposure [60]. Thermoneutral conditions of 30 °C resulted in the attenuation of the anti-obesity effect of capsinoids [60]. Under 17 °C conditions, the capsinoid-treated mice also had significantly lower fasting plasma concentrations of glucose and insulin and improved glucose tolerance and insulin sensitivity as compared to vehicle-treated mice and mice kept at ambient temperature [60].

In humans, oral ingestion of a single 9 mg dose of capsinoids was reported to induce a slight but significant increase in energy expenditure in response to cold exposure (19 °C) in individuals with metabolically active BAT but not in individuals with undetectable BAT as measured by [^{18}F]FDG-PET [61]. Meta-analyses reveal evidence for the therapeutic potential of capsinoids and capsaicin in weight management; however, the thermogenic effects are small and long-term effects are uncertain [62]. It is likely that capsinoids share the same mechanism of action for promoting BAT thermogenesis in humans as has been described in mice – activation

of transient receptor potential vanilloid type 1 (TRPV1) channels in the gastrointestinal tract, which leads to activation the sympathetic nervous system [63]. In mice that lack all three forms of β-adrenergic receptors, the anti-obesity effects of capsinoids were eliminated, suggesting the necessity of the β-adrenergic pathway in capsinoid-stimulated thermogenesis, which could include both direct adrenergic effects and indirect effects via sympathetic nervous system activation [60].

2.1.4.2 Fish Oil

Fish oil is also a dietary component with growing evidence of involvement in BAT regulation. In rats, fish oil supplementation (200 g/kg body weight for 21 days) has been found to increase *Ucp1* mRNA expression in interscapular BAT (iBAT) [64]. Replacement of dietary monounsaturated fats with docosahexaenoic acid (DHA), eicosapentaenoic acid (EPA), or a mixture of DHA and EPA, which are major polyunsaturated fatty acids (PUFA) in fish oil, has been seen to affect mitochondrial and thermogenic activity in the iBAT of rats, with EPA increasing number of mitochondria and DHA or a mixture of DHA and EPA increasing mitochondrial size and activity [65]. In mice, an HFD containing 12% fish oil for 8 weeks was seen to increase mRNA expression of the thermogenic genes *Adrb3, Pgc-1a,* and *Ucp1* in iBAT, prevent diet-induced weight gain, improve glucose tolerance and triglyceride concentrations, and reduce the expression of pro-inflammatory genes [66]. *Pgc-1a, carnitine palmitoyltransferase 1 B (Cpt1b*), and *Prdm16* expression have also been reported to increase in mouse iBAT in response to a fish oil-enriched diet (2.4% DHA- or EPA-enriched fish oil), with no significant changes in *cell death-inducing DFFA-like effector A (Cidea)* or *Fgf21* [67]. While some benefits

of fish oil have been reported in humans, such as improved lipid profiles and glucose homeostasis, little information is available on the role of BAT in these effects [68].

Fish oil may elicit its effect in a similar way as capsaicin and the capsinoids with a mechanism involving TRPV1 and activation of the sympathetic nervous system [67]. In TRPV1 knockout (KO) mice, the anti-obesogenic effects and improvements in plasma glucose and triglyceride concentrations seen with fish oil supplementation in wild-type (WT) mice were lost [67]. Moreover, fish oil resulted in increased norepinephrine in the urine and upregulation of *β_3-AR* mRNA in iBAT in WT mice, but not TRPV1 KO mice, and treatment with a β_3-AR antagonist prevented the fish-oil induced increase in *Ucp1*, suggesting that TRPV1 mediates sympathetic nervous system activation by fish oil, leading to β_3-AR activation and subsequent induction of UCP1 and thermogenesis [67]. Elements of fish oil may impact BAT by other mechanisms. For example, EPA has been shown to induce BAT thermogenesis via FFA receptor 4 (FFAR4) [69].

2.1.4.3 Resveratrol

Another well-known nutritional factor implemented in BAT regulation is resveratrol, a polyphenolic compound found in the weed *Polygonum cuspidatum* and in trace amounts in foods such as red wine and peanuts [70]. High doses of resveratrol of around 400 mg/kg body weight have been shown to decrease weight gain in HFD-fed mice [71, 72]. Increased basal energy expenditure, cold tolerance, mitochondrial volume and DNA, and PGC-1α activity in BAT of mice treated with resveratrol have also been reported [71]. Resveratrol has also been studied in non-human primates (gray mouse lemurs), where it was observed to significantly increase resting energy expenditure [73, 74]. The mechanisms of these effects likely involve AMPK (5'

adenosine monophosphate-activated protein kinase), SIRT1 (Sirtuin 1), and PGC-1α [72]. Resveratrol treatment has been seen to increase *Sirt1* gene expression in mouse BAT which may then deacetylate and increase PGC-1α activity [71, 75]. An increase in phospho-AMPKα was observed in resveratrol treated mice without a difference in total AMPKα, suggesting that resveratrol's effects on BAT are associated with AMPK activation [72]. Also, in differentiated mouse iBAT stromal vascular cells, upregulation PRDM16, UCP1, Cytochrome C, and PDH (pyruvate dehydrogenase) by resveratrol was attenuated by AMPKα1 inhibition or KO, supporting AMPK's role in mediation of resveratrol's effect and providing evidence that the AMPKα1 isoform is responsible [72].

2.1.4.4 Retinoic Acid

Retinoic acid (RA) is a metabolite of vitamin A that can regulate gene expression by binding to retinoic acid receptors (RARs) [76]. The RAR forms a dimer with a retinoid X receptor (RXR), which then regulates gene expression by binding to RA response elements in the promoter regions of target genes [77]. In murine brown adipocytes, RA was found to induce a 7-fold increase in *Ucp1* mRNA levels independently of β-adrenergic pathways and PGC-1α [76]. In mice, a vitamin A-deficient diet resulted in increased body weight, and whole-body fat mass and decreased *Ucp1* expression in iBAT [78]. In mice, treatment with all-trans RA (ATRA) (100 mg/kg body weight) resulted in significant weight loss and increased *Ucp1* expression in iBAT, regardless of whether the mice were on a vitamin A-deficient or regular chow diet [78]. Although RA is a potent positive regulator of BAT activity in mice, similar effects are unlikely in humans based on the observation that ATRA inhibits or has no effect on UCP1 expression in human adipocyte cell lines and primary human white adipocytes [77].

2.1.4.5 Pharmacological Agents

Several pharmacological agents with the ability to regulate BAT activity are also under investigation, many of which mimic nutritional regulators in their mechanisms of action [57]. For example, a specific AMPK activator, A-769662, has been found to activate BAT similarly to resveratrol and is being explored for its therapeutic potential in the treatment of type 2 diabetes [72, 79]. A handful of these drugs have reached human trials, many of which are β_3-AR agonists [8]. β_3-AR agonists are currently used for the treatment of overactive bladder in humans [80]. Of the β_3-AR agonists that have been studied for BAT activation in humans, rafabegron, mirabegron, and ZD2079 have had somewhat positive results. Rafabegron, or TAK-677, promoted a slight increase in energy expenditure at the highest dose (0.5 mg twice daily for 29 days) in obese men and women; however, heart rate was elevated at this dose, and there were no changes in weight, body composition, or fasting insulin, FFA, or glucose concentrations [81]. ZD2079 (600 mg twice daily for 14 days) was studied in obese men and women and was also found to slightly increase energy expenditure [82]. In a study of healthy men, a single dose of 200 mg mirebegron was found to significantly increase BAT metabolic activity as measured by [^{18}F]FDG-PET/CT in all subjects and increase resting metabolic rate by an average of 203 kcal/day [83]. Treatment also increased heart rate and systolic, but not diastolic, blood pressure [83]. These increases were less than what has been reported for other sympathomimetics and there were no unanticipated adverse effects [83, 84]. Cardiovascular side effects are a concern for all β_3-AR agonists since β_3-AR is expressed in the human heart [85].

Pharmacological strategies for increasing norepinephrine are also being explored as a means of increasing BAT activity via adrenergic stimulation. Ephedrine increases

norepinephrine release and acts as an adrenergic receptor agonist itself [86]. In humans, 2.5 mg/kg body weight of ephedrine increased BAT activation as measured by [^{18}F]FDG-PET/CT in lean but not obese individuals, resulting in a mean increase in energy expenditure of 18% in the lean individuals [84]. Ephedrine also significantly increased systolic blood pressure, heart rate, and blood glucose in lean and obese subjects as well as diastolic blood pressure in lean subjects [84]. Atomoxetine is a drug currently marketed for the treatment of attention-deficit/hyperactivity disorder (ADHD) that inhibits norepinephrine reuptake by blocking the presynaptic norepinephrine transporters, thereby prolonging activation of postsynaptic β_3-AR [87]. Rats treated with 0.1 mg/kg body weight of atomoxetine displayed increased [^{18}F]FDG uptake by iBAT, which was significantly blunted by propranolol, a β-adrenergic antagonist [87]. In obese women instructed to follow a calorie-restricted diet, atomoxetine treatment (100 mg/day) resulted in a slightly greater decrease in weight and waist circumference as compared to women receiving a placebo, but the involvement of BAT activity was not investigated [88].

Non-adrenergic regulators of BAT, such as melanocortins, glucocorticoids, natriuretic peptides, and a variety of lipokines, are being investigated as potential therapeutic targets as well [89, 90]. Some of these regulators may be useful applied as pharmacologic agents themselves, while others are being exploited as drugs that mimic the mechanisms of action or manipulate the concentrations of positive regulators of BAT activity [90]. For example, multiple strategies are being used to develop the most effective pharmacological method of increasing circulating levels of FGF21, an endocrine hormone that regulates energy homeostasis and insulin sensitivity which is thought to be at least partly accomplished via BAT regulation [91, 92]. These strategies include PEGylated FGF21, FGF21-antibody conjugates, and antibody-based activation of the

fibroblast growth factor (FGFR)/β-Klotho complex [93-95]. FGF21 analogs LY2405319 and PF-05231023 have been studied in humans. PF-05231023 administration to obese cynomolgus monkeys and human patients with type 2 diabetes resulted in significant weight loss and an improved lipid profile with no significant changes in glucose [94]. Similarly, LY2405319 treatment of obese, diabetic patients showed improvements in lipid levels and fasting insulin and decreased bodyweight with no changes in glucose [96]. While much progress has been made, the development of an effective agent for BAT activation with minimal side effects is an ongoing endeavor that warrants further efforts.

2.2 Overview of sEH Inhibitors

2.2.1 Introduction to sEH

Soluble epoxide hydrolase (sEH) is a homodimeric enzyme with two functionally different domains [97]. The C-terminal domain is a hydrolase that catalyzes the conversion of EpFAs to dihydroxy fatty acids (DiHFAs), also known as diols, while the N-terminal domain is a phosphatase for which neither the endogenous substrate nor physiological role has been fully elucidated [10, 11, 97, 98]. EpFAs include the EETs generated by cytochrome P450 (CYP450) from arachidonic acid as well as the CYP450 products of other polyunsaturated FFAs such as linoleic acid, DHA, and EPA [11, 99]. Many of the EpFAs and their diols are biologically active and affect several biological processes [11, 14, 99-101]. EpFAs can be metabolized by several different pathways, but sEH is the predominant pathway in many tissues [11]. In humans, sEH is encoded by the *EPHX2* gene and expressed widely throughout the body: identified in the liver, kidney, brain, muscles, prostatic ducts, gastrointestinal tract, epithelial cells, and in certain endocrine and lymphatic tissues [102-104]. In some tissues, such as the liver, sEH expression is

broadly distributed while in other tissues, such as the kidney and brain, expression is localized to specific regions [100, 103].

Several factors have been found to regulate sEH expression or activity, with evidence of some tissue-and sex-specific regulation [105-108]. For example, in mice, PPARγ agonists have been seen to induce sEH expression in adipose tissue, but not in the liver, and downregulate sEH in cardiomyocytes [106, 107]. sEH also appears to be regulated by sex hormones, with testosterone increasing and estrogen decreasing sEH activity [109, 110]. Other regulators that have been identified include angiotensin II, reactive oxygen species, homocysteine, and PPARα agonists to name a few [106, 111-115].

2.2.2 sEH and Metabolic Disease

sEH has been studied in relation to a variety of biological processes and disease states [13]. In general, the EpFA precursors of sEH metabolism, especially the EETs, are anti-inflammatory and have a higher biological activity than the diol products of sEH, of which some are actually pro-inflammatory [11, 101]. Because of this, a majority of the current sEH research focuses on the beneficial effects of inhibition of the sEH hydrolase domain [13]. In various animal models, sEH inhibitors (sEHIs) and sEH KO have been found to be protective against many conditions, such as aortic aneurysm, atherosclerosis, stroke, heart attack, arrhythmia, chronic obstructive pulmonary disease, pulmonary hypertension, hypertension-induced organ damage, inflammation, and inflammatory and neuropathic pain [13]. sEH KO and inhibition have also shown to be beneficial for several aspects of metabolic disease [14], which will be discussed further here.

To begin, sEH has been investigated for its role in insulin resistance, a major risk factor in metabolic disease [13, 116-118]. Treatment with the sEHI *t*-AUCB or sEH KO was found to prevent hyperglycemia and augment glucose-stimulated insulin secretion in pancreatic islet cells in mice with streptozotocin-induced diabetes [118]. Diabetic sEH KO mice also had improved glucose tolerance, increased insulin secretion during a hyperglycemic clamp study, and reduced islet cell apoptosis as compared to diabetic WT mice [118]. Another study found that in mice with HFD-induced obesity and type 2 diabetes, sEH KO or inhibition by sEHI TUPS (1-(1-methylsulfonyl-piperidin-4-yl)-3-(4-trifluoromethoxyphenyl)-urea) significantly decreased plasma glucose levels and increased pancreatic islet size and vasculature as compared to WT mice without sEHI treatment [117]. Additionally, sEH KO resulted in increased insulin sensitivity and insulin receptor signaling in the liver [117]. EETs are known to improve insulin resistance, which is thought to be mediated by activation of insulin receptor signaling and adiponectin-mediated AMPK signaling pathways as well as upregulation of nitric oxide synthase expression [14]. This suggests that the observed effects of sEH KO or inhibition on insulin resistance are, at least in part, mediated by the increase in EETs that has been shown to occur with both sEH KO and inhibition in mice [14, 119].

sEH also plays a part in lipid metabolism, another key factor in metabolic disease [120]. In rats fed a high carbohydrate, high fat (HCHF) diet, *t*-AUCB treatment attenuated increases in total cholesterol and non-esterified fatty acids that were seen in control HCHF rats [121]. In adipocytes, *t*-AUCB treatment upregulated ATP-binding cassette transporter A1 (ABCA1), thereby improving cholesterol efflux, and increased CD36-mediated degradation of oxidized LDL (low-density lipoprotein) [121]. In mice, sEH KO was seen to decrease plasma cholesterol

by about 25% and decrease liver expression of HMG-coA reductase by approximately 2-fold as compared to WT mice [119]. Interestingly, further exploration revealed opposite roles of the two sEH domains in regulating cholesterol levels, with overexpression of human sEH phosphatase only in HepG2 cells leading to elevated cholesterol levels, while overexpression of sEH hydrolase only led to lowered cholesterol levels [119]. Consistent with these findings, TUPS treatment of WT mice and HepG2 cells expressing human sEH resulted in elevated cholesterol levels [119].

Non-alcoholic fatty liver disease (NAFLD) is a condition associated with obesity that may benefit from sEH KO or inhibition, which were both shown to alleviate HFD-induced hepatic steatosis in mice [122]. This effect could involve direct inhibition of sEH in the liver as well as the reduction in systemic inflammation observed with sEH inhibition by *t*-AUCB [122]. A more recent study reported similar findings and further added that sEH KO or inhibition with TPPU (1-trifluoromethoxyphenyl-3-(1-propionylpiperidin-4-yl) urea) or *t*-TUCB (*trans*-4-{4-[3-(4-trifluoromethoxy-phenyl)-ureido]-cyclohexyloxy}-benzoic acid) also suppressed expression of genes involved in lipid synthesis and increased expression of *Ppara,* a regulator of β-oxidation, which can explain the suppression of fat accumulation in the liver [123].

Although several studies have demonstrated benefits of sEH inhibition on obesity-associated diseases, the relationship between sEH and obesity itself is less clear [14]. sEH expression increases upon differentiation in both white [106] and brown (unpublished data) adipocytes. Moreover, in vitro and in vivo induction of adipogenesis was seen to decrease adipose-derived EETs, likely indicating increased sEH activity, while administration of stable EET analog (S)-2-(11-(nonyloxy)undec-8(Z)-enamido)succinic acid (NUDSA) or EET-A to

HFD-fed mice resulted in significantly less weight gain, adipose tissue expansion, and mRNA expression of proadipogenic genes in WAT and increased *Ucp1* mRNA expression in BAT [15]. In HFD-fed mice, sEH inhibition by AR9281 1-(1-Acetyl-piperidin-4-yl)-3-adamantan-1-yl-urea) promoted significant weight loss by reducing appetite and increasing metabolic rate, which may be mediated to some degree by BAT, as evidenced by an approximately 50% increase in BAT UCP1 expression in treated mice [16]. However, conflicting results of no effect of sEH inhibition on weight gain in HCHF diet-fed rats or HFD-fed mice have also been reported [121, 122]. These discrepancies may be due to the differences in animal models, sEHI, or doses used.

We have found sEH mRNA to be significantly upregulated in BAT but not epididymal white adipose tissue (eWAT) or inguinal white adipose tissue (iWAT) in HFD-induced obese mice. In vitro studies have revealed that sEH inhibition by *t*-TUCB or *t*-AUCB dose-dependently promotes murine brown adipocyte differentiation (*t*-AUCB more robustly than *t*-TUCB), as demonstrated by lipid accumulation visualized by Oil Red O staining and mRNA and protein expression of brown marker genes UCP1 and PGC-1α (unpublished data).

Taken together, these data support the therapeutic potential of sEH inhibition for metabolic disease. Thorough mechanistic studies of sEHIs and sEH metabolites are still needed so that findings in animal models can be translated to the treatment of human conditions.

2.2.3 sEH Inhibitors

The catalytic activity of the sEH hydrolytic domain has been targeted by mimics of the reaction intermediates and transition states, which serve as inhibitors of the enzyme [10]. A variety of low-nanomolar to picomolar inhibitors were developed following the discovery of dicyclohexyl urea as a reversible sEHI that binds to the sEH active site by mimicking the

reaction intermediate [124, 125]. These inhibitors have a primary urea central pharmacophore and studies of the structure-activity relationship of sEHIs revealed that they should have a small group such as a phenyl or hexyl on one side but can have a larger group on the opposite side [126].

AUDA (12-(3-adamantan-1-yl-ureido) dodecanoic acid), is an sEHI that was designed to mimic fatty acid substrates of sEH and has been found to be a PPARα ligand [22, 25]. AUDA is also rapidly metabolized in vivo due to its susceptibility to CYP450 oxidation and β-oxidation [22]. Even with these limitations, AUDA treatment has yielded positive results in many animal studies [127, 128]. Following the discovery that a polar group called the secondary pharmacophore can be positioned 5-7 atoms from the primary pharmacophore without affecting the potency of the sEHI, sEHIs with improved physical properties were developed [17]. In most of the more recently developed sEH inhibitors, the secondary pharmacophore is typically an ether, as seen in AEPU (1-adamantanyl-3-{5-[2-(2-ethoxyethoxy)ethoxy]pentyl]} urea), a heterocycle, or an amide [17].

The replacement of the alkyl chain present in AUDA and AEPU with a conformationally restricted molecule such as piperdine, cyclohexyl, or phenyl has further improved the potency and pharmacokinetics of sEH inhibitors in multiple species [129]. These inhibitors include TPPU, APAU (1-(1-acetypiperidin-4-yl)-3-adamantanylurea), TPAU (1-trifluoromethoxyphenyl-3-(1-acetylpiperidin-4-yl) urea), *t*-AUCB and its *cis*-isomer *c*-AUCB, *t*-TUCB, sorafenib (4-[4-({[4-chloro-3-(trifluoromethyl)phenyl]carbamoyl}amino)phenoxy]-N-methylpyridine-2-carboxamide), *t*-CUPM (*trans*-4-{4-[3-(4-chloro-3-trifluoromethyl-phenyl)-ureido]-cyclohexyloxy}-pyridine-2-carboxylic acid methylamide) and others [13, 17].

Two sEHIs have entered human clinical trials so far: GSK2256294 ((1R,3S)-N-(4-cyano-2-(trifluoromethyl)benzyl)-3-((4-methyl-6-(methylamino)-1,3,5-triazin-2-yl)amino)cyclohexanecarboxamide), for treatment of diabetes, pulmonary obstructive disease, and subarachnoid hemorrhage, and AR9281, for treatment of hypertension and impaired glucose tolerance [19, 20]. GSK2256294 is an sEHI that has been tested in two phase I trials where it was studied in healthy males, obese male smokers, and healthy elderly males and females for its safety, pharmacokinetics, and effects on biliary metabolites [19]. GSK2256294 (2-20 mg) was well-tolerated with no serious adverse events and demonstrated sustained dose-dependent inhibition of sEH, regardless of age or gender [19]. AR9281 has also been studied in phase I trials in healthy men and women with no serious adverse events and sustained inhibition of sEH when multiple doses (400 mg every 8 hours) were administered [20]. The initial results of these trials, determining that two structurally very different sEHIs are safe for human treatment. However, the efficacy of sEHIs in treating human diseases is yet to be reported.

2.3 sEH Inhibitor *t*-AUCB: Current Applications and Opportunities

2.3.1 *t*-AUCB Structure, Bioavailability, and Efficacy

t-AUCB is one of the more recently developed conformationally restricted sEHIs. The structure of *t*-AUCB is a disubstituted urea central pharmacophore with an *N*-adamantyl group, and an *N'*-trans-1,4 cyclohexane ring serving as a link to benzoic acid. *t*-AUCB was designed in an effort to optimize sEHIs by testing the *trans*- and *cis*-isomers of several different compounds generated by the addition of a polar group to the cyclohexane ring of the base structure N-adamantyl-N′-cyclohexylurea (ACU). *t*-AUCB and *c*-AUCB were found to have dramatically increased water solubility and metabolic stability as well as relatively high inhibitor potencies as

compared to the other compounds developed. In general, the *cis*-isomers tested were less stable than the *trans*-isomers, likely because the *trans*-isomers were less susceptible to metabolism by CYP450s [18].

The pharmacokinetics of the ACU-derived compounds were studied by oral administration of 0.3 mg/kg to dogs, which have been shown to have very similar gastrointestinal absorption to humans [18, 130]. The area under the curve (AUC) estimated for inhibitor plasma concentration versus time was found to be highest for *t*-AUCB, which had a 40-fold increase compared to AUDA and a 4-fold increase compared to APAU[18]. The oral bioavailability of *t*-AUCB was also assessed by comparing plasma concentrations over 24 hours following oral versus intravenous administration in dogs; oral bioavailability was determined to be 98% with a T_{max} of 8 hours and a $T_{1/2}$ of 19 hours [18].

The potency of *t*-AUCB for mouse, rat, hamster, cat, dog, and human sEH was determined by fluorescent or radioactive assays. Unlike other sEHIs, *t*-AUCB was a potent sEHI regardless of the animal species of origin of sEH. Moreover, *t*-AUCB had an IC_{50} of only 2 nM for human sEH. Finally, *t*-AUCB was seen to normalize lipopolysaccharide-induced hypotension in mice with a 10-fold lower dose than what was needed for the prodrug of AUDA, AUDA-BE (12-(3-adamantan-1-ylureido)dodecanoic acid butyl ester), to have similar effects. *t*-AUCB appears to be one of the most promising sEHIs due to its water solubility, stability, bioavailability, and efficacy across species [18].

2.3.2 Current Applications of *t*-AUCB

In addition to the aforementioned metabolic studies that utilized *t*-AUCB for sEH inhibition [2.2.2], *t*-AUCB has been applied to a variety of disease models [131-140]. The effects

of *t*-AUCB on renal function have been studied in rodents [131-134]. In mice, oral administration of *t*-AUCB resulted in fibroprotective and anti-inflammatory effects similar to sEH KO [131, 132]. In rats with streptozotocin-induced diabetes, *t*-AUCB attenuated renal injury by reducing albumin, glomerular albumin permeability, and nephrin excretion while restoring glomerular α3 integrin and nephrin expression [133]. *t*-AUCB treatment of spontaneously hypertensive obese rats reversed the increase in urinary levels of albumin and kidney injury marker-1 (KIM-1) and co-administration of *t*-AUCB with PPARγ agonist rosiglitazone resulted in enhanced reno-protection [134].

The cardiovascular implications of *t*-AUCB have been studied in mice [135, 136]. Infusion of isolated mouse hearts with *t*-AUCB resulted in improved postischemic contractile function and reduced infarct size which was shown to be mediated through EETs and the phosphatidylinositol 3-kinase (PI3K) pathway [135]. In a mouse model of myocardial infarction (MI), treatment with *t*-AUCB for 7 days prior to MI resulted in reduced infarct size, improved cardiac function, prevention of cardiac arrhythmias, and suppression of muscle-specific microRNA-133, a small noncoding RNA that interferes with the expression of arrhythmia-related genes [136].

t-AUCB has also been examined in relation to inflammation [137, 138]. In a lipopolysaccharide-challenged murine model, it was found to enhance the anti-inflammatory effects of aspirin, a cyclooxygenase (COX) inhibitor, or MK886, a 5-lipoxygenase activation protein (FLAP) inhibitor [137]. *t*-AUCB also attenuated the development of inflammatory bowel disease in IL-10 KO mice (a mouse model of IBD), evidenced by a lower incidence of ulcer

formation and transmural inflammation as well as a significant decrease in inflammatory signals and neutrophil infiltration to the bowel [138].

Human studies of *t*-AUCB are still limited to in vitro work. In human glioblastoma cell lines U251 and U87, *t*-AUCB dose-dependently suppressed cell growth, likely via activation of NF-κB [139]. Furthermore, *t*-AUCB treatment induced G0/G1 phase arrest by regulation of Cyclin D1 and phosphorylated-CDC2 levels [139]. In endothelial progenitor cells from patients with acute MI, *t*-AUCB dose-dependently promoted angiogenesis and migration and increased expression of angiogenic factors in a PPARγ-dependent manner [140].

2.3.3 Research Gap

In summary, soluble epoxide hydrolase (sEH) is a cytosolic enzyme that converts epoxy fatty acids (EpFAs) into less active diols. By stabilizing endogenous EpFAs, potent small molecule sEH inhibitors have been shown to be beneficial for many diseases. Two sEHIs have entered human trials and appear to have minimal adverse effects. Our preliminary results have shown that sEH expression was increased during both murine and human brown adipocyte differentiation and that *t*-AUCB treatment dose-dependently induced murine adipocyte differentiation.

The purpose of this thesis is to explore the mechanisms by which *t*-AUCB promotes brown adipogenesis, specifically the role of PPARα and PPARγ in *t*-AUCB-induced brown adipogenesis, to improve our understanding of the inhibitor, its effects reported thus far, and its potential applications.

CHAPTER III
MATERIALS AND METHODS

3.1 Reagents

sEH inhibitor *t*-AUCB was synthesized as previously described [129, 141]. PPARγ antagonist GW9662, PPARα antagonist GW6471, and PPARα agonist WY-14643 were purchased from Cayman Chemical (Ann Arbor, MI). PPARγ agonist rosiglitazone was purchased from Sigma-Aldrich (St. Louis, MO). Dimethyl sulfoxide (DMSO) was purchased from Acros Organics (Thermo Fisher Scientific, Pittsburg, PA). Anti-UCP-1, anti-FABP4, anti-β-Actin, anti-PPARγ, anti-ERK1/2, horseradish peroxidase-conjugated goat anti-rabbit, and horseradish peroxidase-conjugated goat anti-mouse antibodies were purchased from Cell Signaling Technology (Danvers, MA). Anti-PGC-1α antibody was purchased from Millipore (Temecula, CA). Anti-PPARα and anti-α Tubulin antibodies were purchased from Santa Cruz Biotechnology (Dallas, TX). Anti-sEH antibody was generated and used as described previously [142, 143].

3.2 Cell Culture and Differentiation

The murine brown preadipocyte cell line was a gift from Dr. Johannes Klein (University of Lubeck, Lubeck, Germany). This cell line was generated from the interscapular brown fat of newborn C57BL/6 mice [144]. Brown fat cells were maintained in Dulbecco's modified Eagle's medium (DMEM) supplemented with 20% fetal bovine serum (FBS) (Atlanta Biologicals, Flowery Branch, GA) in a humidified 37 °C and 5 % CO_2 incubator until they reached confluence (designated as day 0). The cells were induced to differentiate by treatment with

differentiation media consisting of DMEM supplemented with 20% FBS, 1 nM T3, and 20 nM insulin. Media was replaced every 2 days for 6 days.

Murine sEH WT and sEH KO BAT stromal cells were a gift from Dr. Ahmed Bettaieb (University of Tennessee, Knoxville). Cell lines were generated from mouse primary stromal cells that were isolated from the BAT of sEH (encoded by *Ephx2* gene) WT and KO mice as previously described [145]. The day after isolation (day 1), media was replaced with fresh DMEM supplemented with 20% FBS. On day 3, cells were washed with PBS (phosphate-buffered saline) and media was replaced. Cells were again washed and media changed on day 5. On day 6, cells were trypsinized and reseeded for infection with a lentivirus encoding large T antigen and NeoR gene in crude media for 24 hours. After 24 hours, media was changed back to DMEM with 20% FBS. 48 hours later, media was replaced with selection media of FBS, 20% FBS, and 600 μg neomycin. Cells were maintained in selection media for 2 weeks. For differentiation, the sEH WT and sEH KO cells were grown in DMEM supplemented with 20% FBS until they reached confluence. The cells were induced for 3 days with induction media consisting of differentiation media (DMEM with 20% FBS, 1 nM T3, and 20 nM insulin) supplemented with 0.125 mM indomethacin, 5 μM dexamethasone, and 0.5 mM 3-isobutyl-1-methylxanthine. Cells were then switched to differentiation media for an additional 3 days. Media was replaced every 2 days.

3.3 Lentiviral shRNA Particle Infection

Murine brown preadipocyte cells were plated at ~50% confluence in 6-well plates. The cells were then infected with MISSION Lentiviral Transduction Particles for mouse *Ppara*,

Pparg, or scrambled non-targeting control according to the manufacturer's instructions (Sigma-Aldrich). Stably infected cells were selected by puromycin (40 μg/ml) for two weeks.

3.4 Western Blot Analysis

Total cell lysates were prepared using 1X lysis buffer (Cell Signaling, Danvers, MA) and protein concentrations were determined using the BCA assay kit (Thermo Scientific, Waltham, MA). Proteins were separated on a 10% SDS-PAGE then transferred to polyvinylidene difluoride membranes (Bio-Rad, Hercules, CA). The membranes were blocked in TBST buffer (20 mM Tris Base, 137 mM NaCl, and 0.1% Tween 20 (pH 7.4)) containing 5% nonfat milk. Membranes were then immunoblotted with the indicated primary antibodies at 4°C overnight followed by 1-hour incubation with secondary antibodies conjugated with horseradish peroxidase. Proteins were visualized using ECL Western Blot detection reagent (Pierce, Rockford, IL). Densitometry of bands was quantified using ChemiDocXRS+ imaging system and analyzed using ImageLab software (Bio-Rad).

3.5 RNA Preparation and Quantitative Real-Time PCR Analysis

Total RNA was isolated using TRI reagent (Molecular Research Center, Cincinnati, OH) according to the manufacturer's instructions. Total RNA was quantified using NanoDrop ND-1000 spectrophotometer (NanoDrop Technologies, Wilmington, DE). Reverse transcription was carried out using High Capacity cDNA Reverse Transcription kit (Thermo Scientific, Pittsburgh, PA) according to the manufacturer's instructions. mRNA expression of target genes and the housekeeping gene 36B4 (a ribosomal protein that is a component of the 60S subunit) was measured quantitatively using PowerUp SYBR master mix (Applied Biosystems, Austin TX).

PCR reactions were run in a 96-well format using an ABI 7300HT instrument. Cycle conditions were 50°C 2 min, 95°C 10 min, 40 cycles of 95°C for 15 s, then 60°C for 1 min. Relative gene expression was calculated using the $2^{-\Delta\Delta Ct}$ method, after normalization to the housekeeping gene 36B4. Primer sequences are available upon request.

3.6 Reporter Gene Assays

Murine brown preadipocytes seeded on 24-well plates were transiently transfected with murine PPARγ or PPARα transactivation reporters and β-galactosidase expression plasmid with Lipofectamine 3000 Transfection Reagent and Plus Reagent (Thermo Fisher Scientific, Carlsbad, CA). Murine sEH KO and sEH WT brown preadipocytes were transiently transfected with murine PPARγ or PPARα transactivation reporters and β-galactosidase expression plasmid with Viafect Transfection Reagent (Promega, Madison, WI.). PPARγ transactivation reporters consist of murine PPARγ ligand-binding domain ligated to the Gal4 DNA-binding domain (DBD) (mPPARγ-Gal4) and a reporter construct containing an upstream activating sequence (UAS)–linked luciferase, 4xUAS-TK-luc (TK: thymidine kinase). PPARα transactivation reporters consist of murine PPARα ligand-binding domain ligated to the Gal4 DNA binding domain (DBD) (mPPARα-Gal4) and 4xUAS-TK-luc. Both reporters were gifts from Dr. Susanne Mandrup (University of Southern Denmark, Denmark) [146]. 24 hours post-transfection, the murine brown preadipocytes were treated with vehicle control DMSO or sEH inhibitor *t*-AUCB and DMSO, GW6471, or GW9662 for 18 hours. sEH WT and sEH KO cells were treated with DMSO or *t*-AUCB for 18 hours. Cell lysates were prepared, and reporter luciferase and β-galactosidase activities were measured with GloMax Luminometer (Promega, Madison, WI). Relative luciferase activities were normalized to β-galactosidase activities.

3.7 Statistical Analysis

Statistical analysis was performed using SigmaPlot 14.0 (Systat Software, Inc.). One-way ANOVA with repeated measures followed by multiple group-wise comparisons (Student-NewmanKeuls Method) was performed to determine the differences among the treatment groups (e.g., doses). The level of significance was set at $p < 0.05$.

CHAPTER IV
RESULTS AND DISCUSSION

4.1 Results

4.1.1 Effects of *t*-AUCB on murine brown adipocyte differentiation

First, the effects of *t*-AUCB on murine brown adipocyte differentiation were examined. Lipid accumulation murine brown preadipocytes differentiated in the presence of *t*-AUCB was visualized by Oil Red O staining, which showed a dose-dependent increase in lipid accumulation with *t*-AUCB treatment (Fig. 1B). mRNA expression of marker genes of thermogenesis and differentiation in the differentiated cells was also seen to increase in response to *t*-AUCB in a dose-dependent manner, reaching significant levels for *Pparg* and *Cidea* at 5 μM or above and for *Ucp1*, *Pgc-1a* and *Fabp4* at 10 μM or above (Fig. 1C).

4.1.2 *t*-AUCB activates PPARα, but not PPARγ

To study the roles of PPARs in mediating the observed effects of *t*-AUCB, respective PPAR transactivation reporter assays were performed in a murine brown preadipocyte cell line. In cells transfected with PPARα or PPARγ reporters, *t*-AUCB activated PPARα, but not PPARγ, and this activation was eliminated by cotreatment with PPARα antagonist GW6471 (Fig. 2). PPARγ agonist rosiglitazone produced a ~55-fold increase in PPARγ activation, which was completely attenuated by GW9662 (Fig. 2). There was no activation of PPARα by rosiglitazone (Fig. 2). PPARα agonist WY-14643 produced a ~2.7-fold increase in PPARα activation, which was completely attenuated by GW6471 (Fig. 2). There was no activation of PPARγ by WY-14643.

4.1.3 *t*-AUCB-induced upregulation of mRNA markers of thermogenesis and differentiation is attenuated by PPARα antagonist GW6471.

The role of PPARs in *t*-AUCB's effects was studied using PPAR antagonists. The observed upregulation of *Ucp1*, *Pparg*, *Pgc-1a*, and *Fabp4* in differentiated murine brown adipocytes was attenuated by cotreatment with GW6471, compared to cotreatment with DMSO (Fig. 3). In contrast, GW9662 treatment caused an overall decrease in *Ucp1*, *Pparg*, *Pgc-1a*, and *Fabp4* expression, but the dose-dependent increases of these genes by *t*-AUCB were maintained (Fig 3). Treatment with WY-14643 upregulated *Ucp1*, *Pparg*, *Pgc-1a*, and *Fabp4* to a similar extent as *t*-AUCB, and this upregulation was attenuated by GW6471 and, to a lesser extent, GW9662 (Fig. 3). Rosiglitazone significantly increased *Ucp1, Pgc-1a*, and *Fabp4* expression in DMSO, which was attenuated by GW9662, but enhanced by GW6471 (Fig. 3). *Pparg* expression was significantly decreased with rosiglitazone and DMSO or GW9662 treatment but significantly increased with rosiglitazone and GW6471 (Fig. 3).

4.1.4 *t*-AUCB-induced upregulation of mRNA and protein markers of thermogenesis and differentiation is attenuated by PPARα knockdown.

The role of PPARs in *t*-AUCB's effects were further studied by respective PPAR knockdown. The murine brown preadipocytes were infected with scramble (control), *Ppara* KD, or *Pparg* KD lentivirus, and stable individual KD clones and control clones were selected by antibiotics and expanded for further analysis. The efficiency of knockdown of PPARα and PPARγ was first confirmed by Western Blot analysis. As shown in Fig. 4, a 60-80% decrease in PPARα and PPARγ protein expression was achieved in each of the two selected PPARα KD and PPARγ KD clones, respectively, as compared to the control clones (Fig. 4A). There was no significant difference in average PPARα expression between the PPARγ KD clones and the

control clones, but there was a slight but significant increase in average PPARγ expression in the PPARα KD clones compared to the control clones (Fig. 4A).

PPARα KD and, to a greater extent, PPARγ KD resulted in decreased mRNA expression of *Ucp1*, *Cidea*, and *Pgc-1a* across all treatments as compared to the control (Fig. 4B). *t*-AUCB-induced dose-dependent upregulation of *Ucp1* and *Cidea* was significantly attenuated by PPARα KD and to a greater degree by PPARγ KD as compared to the control (0) of each respective treatment group (Fig. 4B). *t*-AUCB-induced dose-dependent upregulation of *Pgc-1a* and *Fabp4* was almost completely attenuated by PPARα KD but not PPARγ KD (Fig. 4B). Interestingly, PPARγ KD also decreased *Fabp4* expression across all treatments as compared to the control treatment group, but PPARα KD increased *Fabp4* expression by up to nearly 10-fold (Fig. 4B). Upregulation of *Ucp1*, *Cidea*, *Pgc-1a*, and *Fabp4* by WY-14643 was attenuated by PPARα KD (Fig. 4B). With PPARγ KD, WY-14643 still significantly increased expression of *Ucp1*, *Pgc-1a*, and *Fabp4*, but did not significantly affect *Cidea* expression (Fig. 4B). Rosiglitazone significantly increased expression of *Ucp1*, *Cidea*, *Pgc-1a*, and *Fabp4* (Fig. 4B). Upregulation of *Ucp1* and *Cidea* by rosiglitazone was attenuated by PPARγ KD, but upregulation of *Pgc-1a* and *Fabp4* was unchanged and further enhanced, respectively, by PPARγ KD (Fig. 4B). Relative to the control (0) of each treatment group, PPARα KD attenuated rosiglitazone to a greater extent than PPARγ KD in all four genes (Fig. 4B).

Similar patterns were seen in protein expression. PPARα KD, to a greater extent than PPARγ KD, attenuated upregulation of UCP1, PGC-1α, and FABP4 by *t*-AUCB (Fig. 4C). Relative to the control (0) of each treatment group, PPARα KD completely eliminated *t*-AUCB-induced upregulation of PGC-1α and FABP4 (Fig. 4C). An increase in UCP1 with *t*-AUCB was

still evident with PPARα KD, but the degree of UCP1 stimulation by *t*-AUCB with PPARα KD was much less than with PPARγ KD (Fig. 4C). FABP4 protein expression, like mRNA expression, was significantly increased with PPARα KD across all treatments as compared to the control treatment group (Fig. 4C).

4.1.5 *t*-AUCB activates PPARα independent of sEH.

To further understand the mechanisms underlying *t*-AUCB's effects, the response to *t*-AUCB was compared between BAT derived stromal cell lines from sEH WT and KO mice. sEH expression in WT cells was significantly greater than KO cells at both day 0 and day 7, with sEH expression in KO cells being only 12% of WT on day 7 (Fig. 5A). There was no difference in Tubulin expression between sEH WT or KO cells at day 0 and the expression was diminished at day 7 in both cell lines, demonstrating similar differentiation capacities between the WT and KO cells (Fig. 5A). WY-14643 and rosiglitazone induced ~ 3-fold increase in PPARα activation and ~18-fold increase in PPARγ activation, respectively, in sEH WT cells (Fig. 5B). *t*-AUCB activated PPARα to a similar extent in sEH WT compared to that in sEH KO cells (Fig. 5B). Consistently, *t*-AUCB did not significantly activate PPARγ in sEH WT or sEH KO cells (Fig. 5B).

4.2 Discussion

Accumulating evidence supports the involvement of sEH in metabolic diseases and the beneficial effects of sEHIs. sEH has been studied in WAT differentiation [106] and obesity [14, 16], but the role of sEH and the effects of its inhibition in brown adipogenesis are not known. To our knowledge, the current study is the first to demonstrate the effects of sEHI *t*-AUCB on

cellular brown adipogenesis and explore the roles of PPARα and PPARγ. Previously reported metabolic effects of *t*-AUCB include improved insulin secretion in mice with streptozotocin-induced diabetes [118], attenuation of increases in total cholesterol in HCHF-fed rats [121], and upregulation of ABCA1 in adipocytes [121]. The mechanisms of the effects of *t*-AUCB, and sEHIs in general, are not well defined [21]. The presumed underlying mechanism of most of the observed sEHI effects is the accumulation of EETs or other biologically active EpFAs that can occur with sEH inhibition [21]. There is evidence of the existence of a high-affinity EET G-protein-coupled receptor, but this has not been fully characterized [147-149]. Several EET receptors and binding sites have been identified, including FABP [150], cannabinoid receptor [151], dopamine receptor [151], prostaglandin E (EP2) receptor [152], PPARα [23], and PPARγ [24]. The ability of EETs to bind PPARα and PPARγ are of particular interest to us, due to the involvement of these transcription factors in adipogenesis.

The ability of EETs to bind PPARs may explain the reported proadipogenic effects in WAT and increases in UCP1 expression in BAT seen with NUDSA or EET-A treatment [153]. PPARα is expressed primarily in the brown adipose tissue, liver, small intestine, skeletal muscle, and heart, while PPARγ is expressed in the placenta, large intestine, liver, macrophages, and other tissues, with expression being highest in white and brown adipose tissues [154, 155]. PPARγ is necessary for and strongly induces both white and brown adipogenesis [39, 40]. PPARγ directly controls genes involved in fundamental adipocyte functions, such as lipid transport and metabolism, insulin signaling, and adipokine production [155]. Although PPARγ is expressed in both WAT and BAT, tissue-specific transcription factors and PPARγ coregulators allow for distinct targeting of each tissue [156]. PPARγ induces UCP1 expression and is required

for β-adrenergic signaling-mediated induction of thermogenesis in brown adipocytes as well [157, 158]. PPARα, while not required for adipogenesis, can also induce significant adipogenesis [40]. Additionally, PPARα is a characteristic marker of the brown phenotype in adipocytes that plays a key role in thermogenesis [159]. PPARα regulates lipid catabolism and thermogenic gene expression via induction of PGC-1α and PRDM16 [159].

We examined the roles of PPARs in *t*-AUCB's demonstrated promotion of brown adipogenesis (Fig. 1). We show that sEH inhibitor *t*-AUCB activates PPARα, but not PPARγ in murine brown preadipocytes (Fig. 2). We also demonstrate that the inhibition or knockdown of PPARα attenuates *t*-AUCB-induced upregulation of markers of thermogenesis and differentiation (Fig. 3-4). Furthermore, we show that PPARα activation by *t*-AUCB is independent of sEH (Fig. 5). These results suggest that PPARα, more so than PPARγ, plays an important role in *t*-AUCB's effects in cellular brown adipogenesis and that these effects may not depend on sEH.

The exact mechanism by which *t*-AUCB activates PPARα warrants further investigation. sEHIs were designed to mimic the epoxide substrates of sEH [22], of which several have been found to activate PPARα [23, 160]. In transient transfection assays conducted in rabbit kidney epithelial cell line RK13 cells. 1 μM of the omega-alcohol of 14,15-EET or a 1:4 mixture of the omega-alcohols of 8,9- and 11,12-EETs activated human and mouse PPARα [23]. Omega-hydroxylated 14,15-EET was reported to bind human PPARα with high affinity, determined by displacement of cis-parinaric acid from the ligand-binding domain [23]. In transactivation assays carried out in human liver carcinoma cell line HepG2 cells. 10 μM 11,12-EET, 11,12-EEZE (a monounsaturated 11,12-EET analog), or 4,15-EET, but not 8,9-EET, activated both PPARα and

PPARγ [160]. 11,12-DHET and 14,15-DHET, the dihydroxyeicosatrienoic acid (DHET) products of EET metabolism by sEH, were also found to activate both PPARα and PPARγ [160]. Furthermore, the EETs and DHETs induced mPPARα/RXRα-specific heterodimerization and subsequent binding to the PPRE site as well as expression of PPARα-responsive genes [160].

Two sEHIs, CUDA and AUDA, have been found to activate PPARα, but not PPARδ or PPARγ, in PPARα transfected COS-7 cells [25]. CUDA also increased the expression of carnitine palmitoyltransferase 1A, a PPARα responsive gene, in HepG2 cells [25]. It was concluded that the ability of these sEHIs to bind and activate PPARα is dependent on the presence of a carboxylic acid group in their structure; two sEHIs without a carboxylic acid group that were tested were not able to activate PPARα [25]. Like CUDA and AUDA, *t*-AUCB contains a C-terminal carboxylic group [18]. Therefore, it is conceivable that *t*-AUCB itself may directly activate PPARα. However, further PPARα binding assays are needed.

It has been reported that in endothelial progenitor cells from patients with acute myocardial infarction, *t*-AUCB positively modulated angiogenesis-related function in a PPARγ-dependent manner [140]. The activation of PPARγ was attributed to *t*-AUCB's inhibition of sEH, leading to an increase in EETs that activate PPARγ [140]. Further evidence was based only on the observation that PPARγ antagonist GW9662 attenuated *t*-AUCB's effects [140]. These data are compatible with what we report here. We also saw some attenuation by GW9662 in our study of *t*-AUCB's induction of mRNA markers of thermogenesis and differentiation (Fig. 3). However, this attenuation was minimal compared to that of PPARα antagonist GW6471 and may be attributable to the ability of GW9662 to also act as a less-potent PPARα antagonist [161].

To our knowledge, we are the first to explore the mechanisms of *t*-AUCB in brown adipogenesis and the first to suggest that a *t*-AUCB-mediated effect is related to *t*-AUCB's sEH-independent activation of PPARα. Our findings are significant for multiple reasons. We show that *t*-AUCB is a promising agent for the promotion of brown adipogenesis and may, therefore, have therapeutic potential for obesity and obesity-related diseases. Additionally, we demonstrate sEH-independent effects of *t*-AUCB, which may unmask a confounding variable in many studies that presume the effects of *t*-AUCB to be due to sEH inhibition alone. Our findings do not exclude sEH inhibition as a factor in the promotion of brown adipogenesis. Future research is needed to study the effects of sEH metabolites on brown adipogenesis as well as to determine the relative contributions of each mode of action of *t*-AUCB to the promotion of brown adipogenesis.

REFERENCES

1. WHO. *Global Health Observatory (GHO) data*. 2018 [cited 2018 March 22, 2018]; Available from: http://www.who.int/gho/ncd/risk_factors/obesity_text/en/.
2. Lidell, M.E. and S. Enerback, *Brown adipose tissue - a new role in humans?* Nat Rev Endocrinol, 2010. **6**(6): p. 319-325.
3. Cannon, B. and J.A.N. Nedergaard, *Brown Adipose Tissue: Function and Physiological Significance.* Physiological Reviews, 2004. **84**(1): p. 277.
4. Frontini, A. and S. Cinti, *Distribution and development of brown adipocytes in the murine and human adipose organ.* Cell Metab, 2010. **11**(4): p. 253-6.
5. Saito, M., et al., *High incidence of metabolically active brown adipose tissue in healthy adult humans: effects of cold exposure and adiposity.* Diabetes, 2009. **58**(7): p. 1526-31.
6. Chondronikola, M., et al., *Brown Adipose Tissue Improves Whole-Body Glucose Homeostasis and Insulin Sensitivity in Humans.* Diabetes, 2014. **63**(12): p. 4089-4099.
7. Bartelt, A., et al., *Brown adipose tissue activity controls triglyceride clearance.* Nat Med, 2011. **17**(2): p. 200-205.
8. Mukherjee, J., A. Baranwal, and K.N. Schade, *Classification of Therapeutic and Experimental Drugs for Brown Adipose Tissue Activation: Potential Treatment Strategies for Diabetes and Obesity.* Curr Diabetes Rev, 2016. **12**(4): p. 414-428.
9. Okla, M., et al., *Dietary Factors Promoting Brown and Beige Fat Development and Thermogenesis.* Adv Nutr, 2017. **8**(3): p. 473-483.
10. Morisseau, C. and B.D. Hammock, *Epoxide hydrolases: mechanisms, inhibitor designs, and biological roles.* Annu Rev Pharmacol Toxicol, 2005. **45**: p. 311-33.
11. Spector, A.A., *Arachidonic acid cytochrome P450 epoxygenase pathway.* J Lipid Res, 2009. **50 Suppl**: p. S52-6.
12. Bettaieb, A., et al., *Soluble epoxide hydrolase deficiency or inhibition attenuates diet-induced endoplasmic reticulum stress in liver and adipose tissue.* J Biol Chem, 2013. **288**(20): p. 14189-99.
13. Morisseau, C. and B.D. Hammock, *Impact of soluble epoxide hydrolase and epoxyeicosanoids on human health.* Annu Rev Pharmacol Toxicol, 2013. **53**: p. 37-58.
14. Xu, X., et al., *The Role of Cytochrome P450 Epoxygenases, Soluble Epoxide Hydrolase, and Epoxyeicosatrienoic Acids in Metabolic Diseases.* Advances in Nutrition, 2016. **7**(6): p. 1122-1128.
15. Zha, W., et al., *Functional characterization of cytochrome P450-derived epoxyeicosatrienoic acids in adipogenesis and obesity.* J Lipid Res, 2014. **55**(10): p. 2124-36.
16. do Carmo, J.M., et al., *Inhibition of soluble epoxide hydrolase reduces food intake and increases metabolic rate in obese mice.* Nutr Metab Cardiovasc Dis, 2012. **22**(7): p. 598-604.
17. Kim, I.H., et al., *Design, synthesis, and biological activity of 1,3-disubstituted ureas as potent inhibitors of the soluble epoxide hydrolase of increased water solubility.* J Med Chem, 2004. **47**(8): p. 2110-22.
18. Hwang, S.H., et al., *Orally bioavailable potent soluble epoxide hydrolase inhibitors.* J Med Chem, 2007. **50**(16): p. 3825-40.

19. Lazaar, A.L., et al., *Pharmacokinetics, pharmacodynamics and adverse event profile of GSK2256294, a novel soluble epoxide hydrolase inhibitor.* Br J Clin Pharmacol, 2016. **81**(5): p. 971-9.
20. Chen, D., et al., *Pharmacokinetics and pharmacodynamics of AR9281, an inhibitor of soluble epoxide hydrolase, in single- and multiple-dose studies in healthy human subjects.* J Clin Pharmacol, 2012. **52**(3): p. 319-28.
21. He, J., et al., *Soluble epoxide hydrolase: A potential target for metabolic diseases.* J Diabetes, 2016. **8**(3): p. 305-13.
22. Olearczyk, J.J., et al., *Substituted adamantyl-urea inhibitors of the soluble epoxide hydrolase dilate mesenteric resistance vessels.* J Pharmacol Exp Ther, 2006. **318**(3): p. 1307-14.
23. Cowart, L.A., et al., *The CYP4A isoforms hydroxylate epoxyeicosatrienoic acids to form high affinity peroxisome proliferator-activated receptor ligands.* J Biol Chem, 2002. **277**(38): p. 35105-12.
24. Liu, Y., et al., *The antiinflammatory effect of laminar flow: the role of PPARgamma, epoxyeicosatrienoic acids, and soluble epoxide hydrolase.* Proc Natl Acad Sci U S A, 2005. **102**(46): p. 16747-52.
25. Fang, X., et al., *Activation of peroxisome proliferator-activated receptor alpha by substituted urea-derived soluble epoxide hydrolase inhibitors.* J Pharmacol Exp Ther, 2005. **314**(1): p. 260-70.
26. Sacks, H. and M.E. Symonds, *Anatomical locations of human brown adipose tissue: functional relevance and implications in obesity and type 2 diabetes.* Diabetes, 2013. **62**(6): p. 1783-90.
27. Harms, M. and P. Seale, *Brown and beige fat: development, function and therapeutic potential.* Nat Med, 2013. **19**(10): p. 1252-1263.
28. Villarroya, F., et al., *Brown adipose tissue as a secretory organ.* Nat Rev Endocrinol, 2017. **13**(1): p. 26-35.
29. Fitzgibbons, T.P., et al., *Similarity of mouse perivascular and brown adipose tissues and their resistance to diet-induced inflammation.* Am J Physiol Heart Circ Physiol, 2011. **301**(4): p. H1425-37.
30. Ortega, M.T., et al., *Evaluation of macrophage plasticity in brown and white adipose tissue.* Cell Immunol, 2011. **271**(1): p. 124-33.
31. Chondronikola, M., et al., *Brown Adipose Tissue Activation Is Linked to Distinct Systemic Effects on Lipid Metabolism in Humans.* Cell Metabolism, 2016. **23**(6): p. 1200-1206.
32. Thoonen, R., et al., *Functional brown adipose tissue limits cardiomyocyte injury and adverse remodeling in catecholamine-induced cardiomyopathy.* J Mol Cell Cardiol, 2015. **84**: p. 202-11.
33. Schlein, C., et al., *FGF21 Lowers Plasma Triglycerides by Accelerating Lipoprotein Catabolism in White and Brown Adipose Tissues.* Cell Metab, 2016. **23**(3): p. 441-53.
34. Ruan, C.C., et al., *A2A Receptor Activation Attenuates Hypertensive Cardiac Remodeling via Promoting Brown Adipose Tissue-Derived FGF21.* Cell Metab, 2018. **28**(3): p. 476-489.e5.

35. Egecioglu, E., et al., *Interleukin-6 is important for regulation of core body temperature during long-term cold exposure in mice.* Biomed Rep, 2018. **9**(3): p. 206-212.
36. Townsend, K. and Y.H. Tseng, *Brown adipose tissue: Recent insights into development, metabolic function and therapeutic potential.* Adipocyte, 2012. **1**(1): p. 13-24.
37. Seale, P., et al., *PRDM16 controls a brown fat/skeletal muscle switch.* Nature, 2008. **454**(7207): p. 961-7.
38. Sanchez-Gurmaches, J., et al., *PTEN loss in the Myf5 lineage redistributes body fat and reveals subsets of white adipocytes that arise from Myf5 precursors.* Cell Metab, 2012. **16**(3): p. 348-62.
39. Floyd, Z.E. and J.M. Stephens, *Controlling a master switch of adipocyte development and insulin sensitivity: covalent modifications of PPARgamma.* Biochim Biophys Acta, 2012. **1822**(7): p. 1090-5.
40. Brun, R.P., et al., *Differential activation of adipogenesis by multiple PPAR isoforms.* Genes Dev, 1996. **10**(8): p. 974-84.
41. Kajimura, S., et al., *Initiation of myoblast to brown fat switch by a PRDM16-C/EBP-beta transcriptional complex.* Nature, 2009. **460**(7259): p. 1154-8.
42. Seale, P., et al., *Transcriptional control of brown fat determination by PRDM16.* Cell Metab, 2007. **6**(1): p. 38-54.
43. Cao, W., et al., *p38 mitogen-activated protein kinase is the central regulator of cyclic AMP-dependent transcription of the brown fat uncoupling protein 1 gene.* Mol Cell Biol, 2004. **24**(7): p. 3057-67.
44. Puigserver, P., et al., *A cold-inducible coactivator of nuclear receptors linked to adaptive thermogenesis.* Cell, 1998. **92**(6): p. 829-39.
45. Lin, J., C. Handschin, and B.M. Spiegelman, *Metabolic control through the PGC-1 family of transcription coactivators.* Cell Metab, 2005. **1**(6): p. 361-70.
46. Rothwell, N.J. and M.J. Stock, *Luxuskonsumption, Diet-Induced Thermogenesis and Brown Fat: The Case in Favour.* Clinical Science, 1983. **64**(1): p. 19.
47. Yoneshiro, T., et al., *Recruited brown adipose tissue as an antiobesity agent in humans.* J Clin Invest, 2013. **123**(8): p. 3404-8.
48. Hanssen, M.J., et al., *Short-term cold acclimation improves insulin sensitivity in patients with type 2 diabetes mellitus.* Nat Med, 2015. **21**(8): p. 863-5.
49. Hanssen, M.J., et al., *Short-term Cold Acclimation Recruits Brown Adipose Tissue in Obese Humans.* Diabetes, 2016. **65**(5): p. 1179-89.
50. Lee, P., et al., *Temperature-acclimated brown adipose tissue modulates insulin sensitivity in humans.* Diabetes, 2014. **63**(11): p. 3686-98.
51. Orava, J., et al., *Different metabolic responses of human brown adipose tissue to activation by cold and insulin.* Cell Metab, 2011. **14**(2): p. 272-9.
52. Berbée, J.F.P., et al., *Brown fat activation reduces hypercholesterolaemia and protects from atherosclerosis development.* Nature Communications, 2015. **6**: p. 6356.
53. Ouellet, V., et al., *Outdoor temperature, age, sex, body mass index, and diabetic status determine the prevalence, mass, and glucose-uptake activity of 18F-FDG-detected BAT in humans.* J Clin Endocrinol Metab, 2011. **96**(1): p. 192-9.
54. Voets, T., et al., *The principle of temperature-dependent gating in cold- and heat-sensitive TRP channels.* Nature, 2004. **430**(7001): p. 748-754.

55. Hoeke, G., et al., *Role of Brown Fat in Lipoprotein Metabolism and Atherosclerosis.* Circ Res, 2016. **118**(1): p. 173-82.
56. Bartness, T.J., C.H. Vaughan, and C.K. Song, *Sympathetic and sensory innervation of brown adipose tissue.* Int J Obes (Lond), 2010. **34 Suppl 1**: p. S36-42.
57. Haas, B., et al., *Targeting adipose tissue.* Diabetol Metab Syndr, 2012. **4**(1): p. 43.
58. Schreiber, R., et al., *Cold-Induced Thermogenesis Depends on ATGL-Mediated Lipolysis in Cardiac Muscle, but Not Brown Adipose Tissue.* Cell Metab, 2017. **26**(5): p. 753-763.e7.
59. Shin, H., et al., *Lipolysis in Brown Adipocytes Is Not Essential for Cold-Induced Thermogenesis in Mice.* Cell Metab, 2017. **26**(5): p. 764-777.e5.
60. Ohyama, K., et al., *A Synergistic Antiobesity Effect by a Combination of Capsinoids and Cold Temperature Through Promoting Beige Adipocyte Biogenesis.* Diabetes, 2016. **65**(5): p. 1410-23.
61. Yoneshiro, T., et al., *Nonpungent capsaicin analogs (capsinoids) increase energy expenditure through the activation of brown adipose tissue in humans.* Am J Clin Nutr, 2012. **95**(4): p. 845-50.
62. Ludy, M.J., G.E. Moore, and R.D. Mattes, *The effects of capsaicin and capsiate on energy balance: critical review and meta-analyses of studies in humans.* Chem Senses, 2012. **37**(2): p. 103-21.
63. Ono, K., et al., *Intragastric administration of capsiate, a transient receptor potential channel agonist, triggers thermogenic sympathetic responses.* J Appl Physiol (1985), 2011. **110**(3): p. 789-98.
64. Takahashi, Y. and T. Ide, *Dietary n-3 fatty acids affect mRNA level of brown adipose tissue uncoupling protein 1, and white adipose tissue leptin and glucose transporter 4 in the rat.* Br J Nutr, 2000. **84**(2): p. 175-84.
65. Oudart, H., et al., *Brown fat thermogenesis in rats fed high-fat diets enriched with n-3 polyunsaturated fatty acids.* Int J Obes Relat Metab Disord, 1997. **21**(11): p. 955-62.
66. Bargut, T.C., et al., *Mice fed fish oil diet and upregulation of brown adipose tissue thermogenic markers.* Eur J Nutr, 2016. **55**(1): p. 159-69.
67. Kim, M., et al., *Fish oil intake induces UCP1 upregulation in brown and white adipose tissue via the sympathetic nervous system.* Sci Rep, 2015. **5**: p. 18013.
68. Martinez-Fernandez, L., et al., *Omega-3 fatty acids and adipose tissue function in obesity and metabolic syndrome.* Prostaglandins Other Lipid Mediat, 2015. **121**(Pt A): p. 24-41.
69. Kim, J., et al., *Eicosapentaenoic Acid Potentiates Brown Thermogenesis through FFAR4-dependent Up-regulation of miR-30b and miR-378.* J Biol Chem, 2016. **291**(39): p. 20551-62.
70. Mele, L., et al., *Dietary (Poly)phenols, Brown Adipose Tissue Activation, and Energy Expenditure: A Narrative Review.* Advances in Nutrition, 2017. **8**(5): p. 694-704.
71. Lagouge, M., et al., *Resveratrol improves mitochondrial function and protects against metabolic disease by activating SIRT1 and PGC-1alpha.* Cell, 2006. **127**(6): p. 1109-22.
72. Wang, S., et al., *Resveratrol enhances brown adipocyte formation and function by activating AMP-activated protein kinase (AMPK) alpha1 in mice fed high-fat diet.* Mol Nutr Food Res, 2017. **61**(4).

73. Dal-Pan, A., S. Blanc, and F. Aujard, *Resveratrol suppresses body mass gain in a seasonal non-human primate model of obesity.* BMC Physiol, 2010. **10**: p. 11.
74. Dal-Pan, A., et al., *Caloric restriction or resveratrol supplementation and ageing in a non-human primate: first-year outcome of the RESTRIKAL study in Microcebus murinus.* Age (Dordr), 2011. **33**(1): p. 15-31.
75. Andrade, J.M., et al., *Resveratrol increases brown adipose tissue thermogenesis markers by increasing SIRT1 and energy expenditure and decreasing fat accumulation in adipose tissue of mice fed a standard diet.* Eur J Nutr, 2014. **53**(7): p. 1503-10.
76. Alvarez, R., et al., *A novel regulatory pathway of brown fat thermogenesis. Retinoic acid is a transcriptional activator of the mitochondrial uncoupling protein gene.* J Biol Chem, 1995. **270**(10): p. 5666-73.
77. Murholm, M., et al., *Retinoic acid has different effects on UCP1 expression in mouse and human adipocytes.* BMC Cell Biol, 2013. **14**: p. 41.
78. Bonet, M.L., et al., *Opposite effects of feeding a vitamin A-deficient diet and retinoic acid treatment on brown adipose tissue uncoupling protein 1 (UCP1), UCP2 and leptin expression.* J Endocrinol, 2000. **166**(3): p. 511-7.
79. Desjardins, E.M. and G.R. Steinberg, *Emerging Role of AMPK in Brown and Beige Adipose Tissue (BAT): Implications for Obesity, Insulin Resistance, and Type 2 Diabetes.* Curr Diab Rep, 2018. **18**(10): p. 80.
80. Michel, M.C. and C. Korstanje, *beta3-Adrenoceptor agonists for overactive bladder syndrome: Role of translational pharmacology in a repositioning clinical drug development project.* Pharmacol Ther, 2016. **159**: p. 66-82.
81. Redman, L.M., et al., *Lack of an effect of a novel beta3-adrenoceptor agonist, TAK-677, on energy metabolism in obese individuals: a double-blind, placebo-controlled randomized study.* J Clin Endocrinol Metab, 2007. **92**(2): p. 527-31.
82. Buemann, B., S. Toubro, and A. Astrup, *Effects of the two beta3-agonists, ZD7114 and ZD2079 on 24 hour energy expenditure and respiratory quotient in obese subjects.* Int J Obes Relat Metab Disord, 2000. **24**(12): p. 1553-60.
83. Cypess, A.M., et al., *Activation of human brown adipose tissue by a beta3-adrenergic receptor agonist.* Cell Metab, 2015. **21**(1): p. 33-8.
84. Carey, A.L., et al., *Ephedrine activates brown adipose tissue in lean but not obese humans.* Diabetologia, 2013. **56**(1): p. 147-55.
85. Lucia, C.d., A. Eguchi, and W.J. Koch, *New Insights in Cardiac β-Adrenergic Signaling During Heart Failure and Aging.* Frontiers in Pharmacology, 2018. **9**: p. 904.
86. Dulloo, A.G., J. Seydoux, and L. Girardier, *Peripheral mechanisms of thermogenesis induced by ephedrine and caffeine in brown adipose tissue.* Int J Obes, 1991. **15**(5): p. 317-26.
87. Mirbolooki, M.R., et al., *Targeting presynaptic norepinephrine transporter in brown adipose tissue: a novel imaging approach and potential treatment for diabetes and obesity.* Synapse, 2013. **67**(2): p. 79-93.
88. Gadde, K.M., et al., *Atomoxetine for weight reduction in obese women: a preliminary randomised controlled trial.* International Journal of Obesity, 2006. **30**(7): p. 1138-1142.
89. Braun, K., et al., *Non-adrenergic control of lipolysis and thermogenesis in adipose tissues.* J Exp Biol, 2018. **221**(Pt Suppl 1).

90. Lynes, M.D., S.D. Kodani, and Y.-H. Tseng, *Lipokines and Thermogenesis.* Endocrinology, 2019.
91. Zhang, J. and Y. Li, *Fibroblast growth factor 21, the endocrine FGF pathway and novel treatments for metabolic syndrome.* Drug Discov Today, 2014. **19**(5): p. 579-89.
92. BonDurant, L.D., et al., *FGF21 Regulates Metabolism Through Adipose-Dependent and -Independent Mechanisms.* Cell Metabolism, 2017. **25**(4): p. 935-944.e4.
93. Ye, X., et al., *Long-lasting anti-diabetic efficacy of PEGylated FGF-21 and liraglutide in treatment of type 2 diabetic mice.* Endocrine, 2015. **49**(3): p. 683-92.
94. Talukdar, S., et al., *A Long-Acting FGF21 Molecule, PF-05231023, Decreases Body Weight and Improves Lipid Profile in Non-human Primates and Type 2 Diabetic Subjects.* Cell Metab, 2016. **23**(3): p. 427-40.
95. Reitman, M.L., *FGF21 mimetic shows therapeutic promise.* Cell Metab, 2013. **18**(3): p. 307-9.
96. Gaich, G., et al., *The effects of LY2405319, an FGF21 analog, in obese human subjects with type 2 diabetes.* Cell Metab, 2013. **18**(3): p. 333-40.
97. Arand, M., et al., *The telltale structures of epoxide hydrolases.* Drug Metab Rev, 2003. **35**(4): p. 365-83.
98. Kramer, J. and E. Proschak, *Phosphatase activity of soluble epoxide hydrolase.* Prostaglandins Other Lipid Mediat, 2017. **133**: p. 88-92.
99. Morisseau, C., et al., *Naturally occurring monoepoxides of eicosapentaenoic acid and docosahexaenoic acid are bioactive antihyperalgesic lipids.* J Lipid Res, 2010. **51**(12): p. 3481-90.
100. Yu, Z., et al., *Vascular localization of soluble epoxide hydrolase in the human kidney.* Am J Physiol Renal Physiol, 2004. **286**(4): p. F720-6.
101. Viswanathan, S., et al., *Involvement of CYP 2C9 in mediating the proinflammatory effects of linoleic acid in vascular endothelial cells.* J Am Coll Nutr, 2003. **22**(6): p. 502-10.
102. Ahmed, E.E., et al., *Distribution of Soluble Epoxide Hydrolase and of Cytochrome P450 2C8, 2C9, and 2J2 in Human Tissues.* Journal of Histochemistry & Cytochemistry, 2004. **52**(4): p. 447-454.
103. Sura, P., et al., *Distribution and expression of soluble epoxide hydrolase in human brain.* J Histochem Cytochem, 2008. **56**(6): p. 551-9.
104. Decker, M., M. Arand, and A. Cronin, *Mammalian epoxide hydrolases in xenobiotic metabolism and signalling.* Arch Toxicol, 2009. **83**(4): p. 297-318.
105. Newman, J.W., C. Morisseau, and B.D. Hammock, *Epoxide hydrolases: their roles and interactions with lipid metabolism.* Prog Lipid Res, 2005. **44**(1): p. 1-51.
106. De Taeye, B.M., et al., *Expression and regulation of soluble epoxide hydrolase in adipose tissue.* Obesity (Silver Spring), 2010. **18**(3): p. 489-98.
107. Pang, W., et al., *Activation of peroxisome proliferator-activated receptor-gamma downregulates soluble epoxide hydrolase in cardiomyocytes.* Clin Exp Pharmacol Physiol, 2011. **38**(6): p. 358-64.
108. Harris, T.R. and B.D. Hammock, *Soluble epoxide hydrolase: gene structure, expression and deletion.* Gene, 2013. **526**(2): p. 61-74.

109. Pinot, F., et al., *Differential regulation of soluble epoxide hydrolase by clofibrate and sexual hormones in the liver and kidneys of mice.* Biochem Pharmacol, 1995. **50**(4): p. 501-8.
110. Yang, Y.-M., et al., *Estrogen-dependent epigenetic regulation of soluble epoxide hydrolase via DNA methylation.* Proceedings of the National Academy of Sciences, 2018. **115**(3): p. 613.
111. Ai, D., et al., *Angiotensin II up-regulates soluble epoxide hydrolase in vascular endothelium in vitro and in vivo.* Proc Natl Acad Sci U S A, 2007. **104**(21): p. 9018-23.
112. Ai, D., et al., *Soluble epoxide hydrolase plays an essential role in angiotensin II-induced cardiac hypertrophy.* Proc Natl Acad Sci U S A, 2009. **106**(2): p. 564-9.
113. Zhao, X., et al., *Soluble epoxide hydrolase inhibition protects the kidney from hypertension-induced damage.* J Am Soc Nephrol, 2004. **15**(5): p. 1244-53.
114. Oguro, A., N. Fujita, and S. Imaoka, *Regulation of soluble epoxide hydrolase (sEH) in mice with diabetes: high glucose suppresses sEH expression.* Drug Metab Pharmacokinet, 2009. **24**(5): p. 438-45.
115. Zhang, D., et al., *Homocysteine upregulates soluble epoxide hydrolase in vascular endothelium in vitro and in vivo.* Circ Res, 2012. **110**(6): p. 808-17.
116. Guo, S., *Insulin signaling, resistance, and the metabolic syndrome: insights from mouse models into disease mechanisms.* J Endocrinol, 2014. **220**(2): p. T1-t23.
117. Luria, A., et al., *Soluble epoxide hydrolase deficiency alters pancreatic islet size and improves glucose homeostasis in a model of insulin resistance.* Proc Natl Acad Sci U S A, 2011. **108**(22): p. 9038-43.
118. Luo, P., et al., *Inhibition or deletion of soluble epoxide hydrolase prevents hyperglycemia, promotes insulin secretion, and reduces islet apoptosis.* J Pharmacol Exp Ther, 2010. **334**(2): p. 430-8.
119. EnayetAllah, A.E., et al., *Opposite regulation of cholesterol levels by the phosphatase and hydrolase domains of soluble epoxide hydrolase.* J Biol Chem, 2008. **283**(52): p. 36592-8.
120. Lee, C.-H., P. Olson, and R.M. Evans, *Minireview: Lipid Metabolism, Metabolic Diseases, and Peroxisome Proliferator-Activated Receptors.* Endocrinology, 2003. **144**(6): p. 2201-2207.
121. Iyer, A., et al., *Pharmacological inhibition of soluble epoxide hydrolase ameliorates diet-induced metabolic syndrome in rats.* Exp Diabetes Res, 2012. **2012**: p. 758614.
122. Liu, Y., et al., *Inhibition of soluble epoxide hydrolase attenuates high-fat-diet-induced hepatic steatosis by reduced systemic inflammatory status in mice.* PLoS One, 2012. **7**(6): p. e39165.
123. Zhang, J., et al., *Pharmacological inhibition or genetic ablation of soluble epoxide hydrolase attenuates obesity-induced nonalcoholic fatty liver disease.* The FASEB Journal, 2018. **32**(1_supplement): p. 560.7-560.7.
124. Shen, H.C. and B.D. Hammock, *Discovery of inhibitors of soluble epoxide hydrolase: a target with multiple potential therapeutic indications.* J Med Chem, 2012. **55**(5): p. 1789-808.
125. Morisseau, C., et al., *Potent urea and carbamate inhibitors of soluble epoxide hydrolases.* Proc Natl Acad Sci U S A, 1999. **96**(16): p. 8849-54.

126. Morisseau, C., et al., *Structural refinement of inhibitors of urea-based soluble epoxide hydrolases.* Biochem Pharmacol, 2002. **63**(9): p. 1599-608.
127. Zhang, J., Y.S. Liu, and Q.H. Lu, *Therapeutic effects of the soluble epoxide hydrolase (sEH) inhibitor AUDA on atherosclerotic diseases.* Pharmazie, 2015. **70**(1): p. 24-8.
128. Chang, L.-H., et al., *Blockade of soluble epoxide hydrolase attenuates post-ischemic neuronal hyperexcitation and confers resilience against stroke with TrkB activation.* Scientific Reports, 2018. **8**(1): p. 118.
129. Tsai, H.J., et al., *Pharmacokinetic screening of soluble epoxide hydrolase inhibitors in dogs.* Eur J Pharm Sci, 2010. **40**(3): p. 222-38.
130. Jezyk, N., W. Rubas, and G.M. Grass, *Permeability characteristics of various intestinal regions of rabbit, dog, and monkey.* Pharm Res, 1992. **9**(12): p. 1580-6.
131. Kim, J., et al., *Inhibition of soluble epoxide hydrolase prevents renal interstitial fibrosis and inflammation.* Am J Physiol Renal Physiol, 2014. **307**(8): p. F971-80.
132. Kim, J., et al., *Pharmacological inhibition of soluble epoxide hydrolase prevents renal interstitial fibrogenesis in obstructive nephropathy.* Am J Physiol Renal Physiol, 2015. **308**(2): p. F131-9.
133. Katary, M.M., C. Pye, and A.A. Elmarakby, *Meloxicam fails to augment the reno-protective effects of soluble epoxide hydrolase inhibition in streptozotocin-induced diabetic rats via increased 20-HETE levels.* Prostaglandins Other Lipid Mediat, 2017. **132**: p. 3-11.
134. Imig, J.D., et al., *Soluble epoxide hydrolase inhibition and peroxisome proliferator activated receptor gamma agonist improve vascular function and decrease renal injury in hypertensive obese rats.* Exp Biol Med (Maywood), 2012. **237**(12): p. 1402-12.
135. Chaudhary, K.R., et al., *Inhibition of soluble epoxide hydrolase by trans-4- [4-(3-adamantan-1-yl-ureido)-cyclohexyloxy]-benzoic acid is protective against ischemia-reperfusion injury.* J Cardiovasc Pharmacol, 2010. **55**(1): p. 67-73.
136. Gui, Y., et al., *Soluble epoxide hydrolase inhibitors, t-AUCB, downregulated miR-133 in a mouse model of myocardial infarction.* Lipids Health Dis, 2018. **17**(1): p. 129.
137. Liu, J.-Y., et al., *Inhibition of soluble epoxide hydrolase enhances the anti-inflammatory effects of aspirin and 5-lipoxygenase activation protein inhibitor in a murine model.* Biochemical Pharmacology, 2010. **79**(6): p. 880-887.
138. Zhang, W., et al., *Soluble epoxide hydrolase gene deficiency or inhibition attenuates chronic active inflammatory bowel disease in IL-10(-/-) mice.* Dig Dis Sci, 2012. **57**(10): p. 2580-91.
139. Li, J., et al., *t-AUCB, an improved sEH inhibitor, suppresses human glioblastoma cell growth by activating NF-kappaB-p65.* J Neurooncol, 2012. **108**(3): p. 385-93.
140. Xu, D.Y., et al., *A potent soluble epoxide hydrolase inhibitor, t-AUCB, acts through PPARgamma to modulate the function of endothelial progenitor cells from patients with acute myocardial infarction.* Int J Cardiol, 2013. **167**(4): p. 1298-304.
141. Rose, T.E., et al., *1-Aryl-3-(1-acylpiperidin-4-yl)urea inhibitors of human and murine soluble epoxide hydrolase: structure-activity relationships, pharmacokinetics, and reduction of inflammatory pain.* J Med Chem, 2010. **53**(19): p. 7067-75.

142. Ren, Q., et al., *Gene deficiency and pharmacological inhibition of soluble epoxide hydrolase confers resilience to repeated social defeat stress.* Proc Natl Acad Sci U S A, 2016. **113**(13): p. E1944-52.
143. Bettaieb, A., et al., *Soluble epoxide hydrolase in podocytes is a significant contributor to renal function under hyperglycemia.* Biochim Biophys Acta Gen Subj, 2017. **1861**(11 Pt A): p. 2758-2765.
144. Klein, J., et al., *Novel adipocyte lines from brown fat: a model system for the study of differentiation, energy metabolism, and insulin action.* Bioessays, 2002. **24**(4): p. 382-8.
145. Hausman, D.B., H.J. Park, and G.J. Hausman, *Isolation and culture of preadipocytes from rodent white adipose tissue.* Methods Mol Biol, 2008. **456**: p. 201-19.
146. Taxvig, C., et al., *Differential effects of environmental chemicals and food contaminants on adipogenesis, biomarker release and PPARgamma activation.* Mol Cell Endocrinol, 2012. **361**(1-2): p. 106-15.
147. Liu, X., et al., *Functional screening for G protein-coupled receptor targets of 14,15-epoxyeicosatrienoic acid.* Prostaglandins Other Lipid Mediat, 2017. **132**: p. 31-40.
148. Chen, Y., et al., *20-Iodo-14,15-epoxyeicosa-8(Z)-enoyl-3-azidophenylsulfonamide: photoaffinity labeling of a 14,15-epoxyeicosatrienoic acid receptor.* Biochemistry, 2011. **50**(18): p. 3840-8.
149. Lahvic, J.L., et al., *Specific oxylipins enhance vertebrate hematopoiesis via the receptor GPR132.* Proc Natl Acad Sci U S A, 2018. **115**(37): p. 9252-9257.
150. Widstrom, R.L., A.W. Norris, and A.A. Spector, *Binding of cytochrome P450 monooxygenase and lipoxygenase pathway products by heart fatty acid-binding protein.* Biochemistry, 2001. **40**(4): p. 1070-6.
151. Inceoglu, B., et al., *Soluble epoxide hydrolase inhibition reveals novel biological functions of epoxyeicosatrienoic acids (EETs).* Prostaglandins Other Lipid Mediat, 2007. **82**(1-4): p. 42-9.
152. Yang, C., et al., *14,15-Epoxyeicosatrienoic acid induces vasorelaxation through the prostaglandin EP(2) receptors in rat mesenteric artery.* Prostaglandins Other Lipid Mediat, 2010. **93**(1-2): p. 44-51.
153. Zha, W., et al., *Functional characterization of cytochrome P450-derived epoxyeicosatrienoic acids in adipogenesis and obesity.* Journal of Lipid Research, 2014. **55**(10): p. 2124-2136.
154. Grimaldi, P.A., *The roles of PPARs in adipocyte differentiation.* Progress in Lipid Research, 2001. **40**(4): p. 269-281.
155. Lehrke, M. and M.A. Lazar, *The many faces of PPARgamma.* Cell, 2005. **123**(6): p. 993-9.
156. Koppen, A. and E. Kalkhoven, *Brown vs white adipocytes: The PPARγ coregulator story.* FEBS Letters, 2010. **584**(15): p. 3250-3259.
157. Lasar, D., et al., *Peroxisome Proliferator Activated Receptor Gamma Controls Mature Brown Adipocyte Inducibility through Glycerol Kinase.* Cell Rep, 2018. **22**(3): p. 760-773.
158. Sears, I.B., et al., *Differentiation-dependent expression of the brown adipocyte uncoupling protein gene: regulation by peroxisome proliferator-activated receptor gamma.* Molecular and Cellular Biology, 1996. **16**(7): p. 3410.

159. Hondares, E., et al., *Peroxisome Proliferator-activated Receptor α (PPARα) Induces PPARγ Coactivator 1α (PGC-1α) Gene Expression and Contributes to Thermogenic Activation of Brown Fat: INVOLVEMENT OF PRDM16.* Journal of Biological Chemistry, 2011. **286**(50): p. 43112-43122.
160. Ng, V.Y., et al., *Cytochrome P450 eicosanoids are activators of peroxisome proliferator-activated receptor alpha.* Drug Metab Dispos, 2007. **35**(7): p. 1126-34.
161. Leesnitzer, L.M., et al., *Functional consequences of cysteine modification in the ligand binding sites of peroxisome proliferator activated receptors by GW9662.* Biochemistry, 2002. **41**(21): p. 6640-50.

APPENDIX

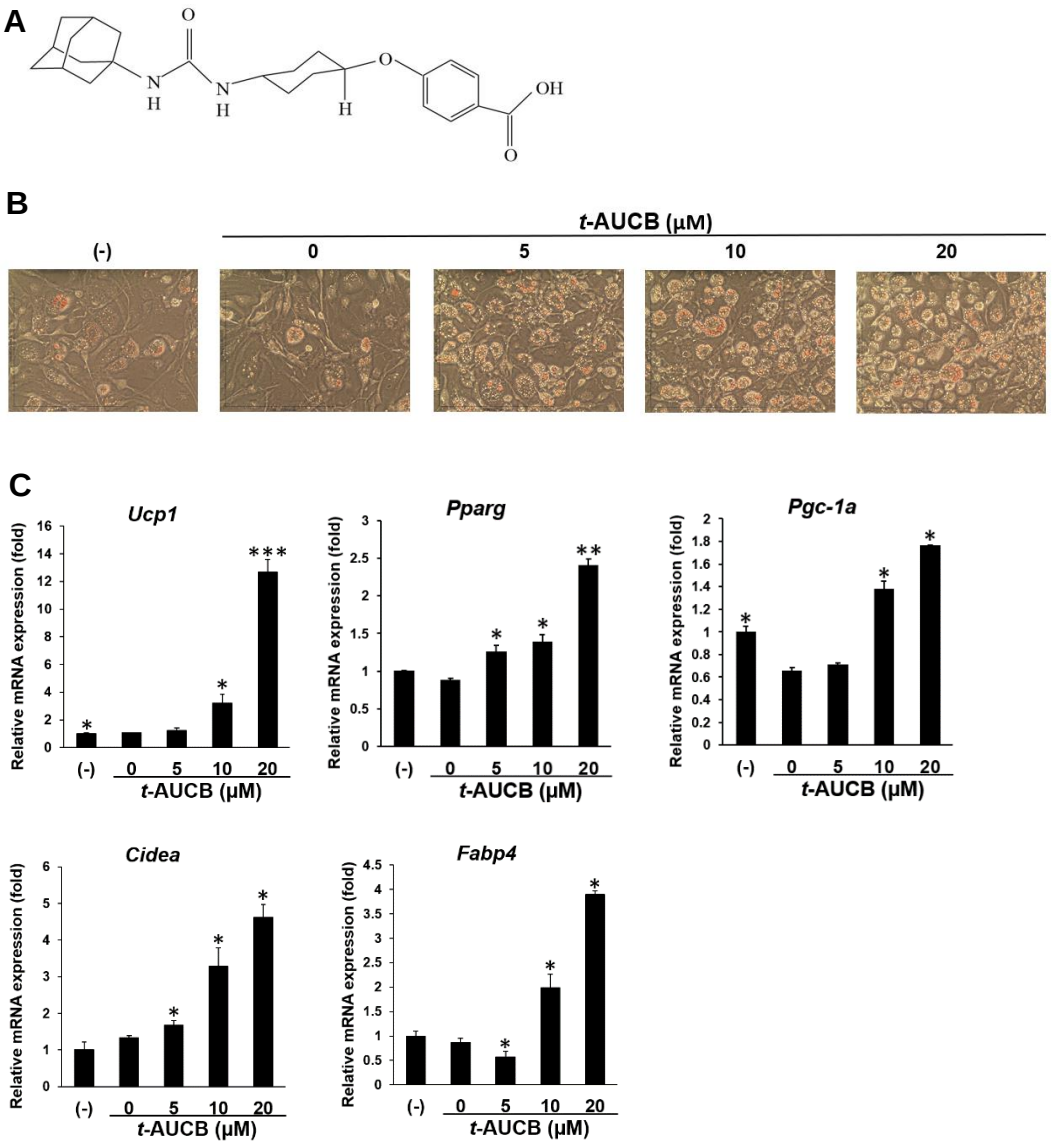

Figure 1. sEH inhibitor *t*-AUCB promotes murine brown adipocyte differentiation.

Murine brown preadipocytes were differentiated in the presence of *t*-AUCB (0, 5, 10, 20 μM) for 6 days. Total RNA samples were isolated and cells were stained on day 6. (A) Chemical structure of *t*-AUCB is shown. (B) Oil red O stained cell morphology is shown. (C) mRNA expression of brown marker genes *Ucp1*, *Pparg*, *Pgc-1a*, and *Cidea* and general differentiation marker *Fabp4* are shown. Data=Mean±SEM (n=3). *, **, ***, $p<0.05$, $p<0.01$, and $p<0.001$, respectively, as compared to the control sample (0).

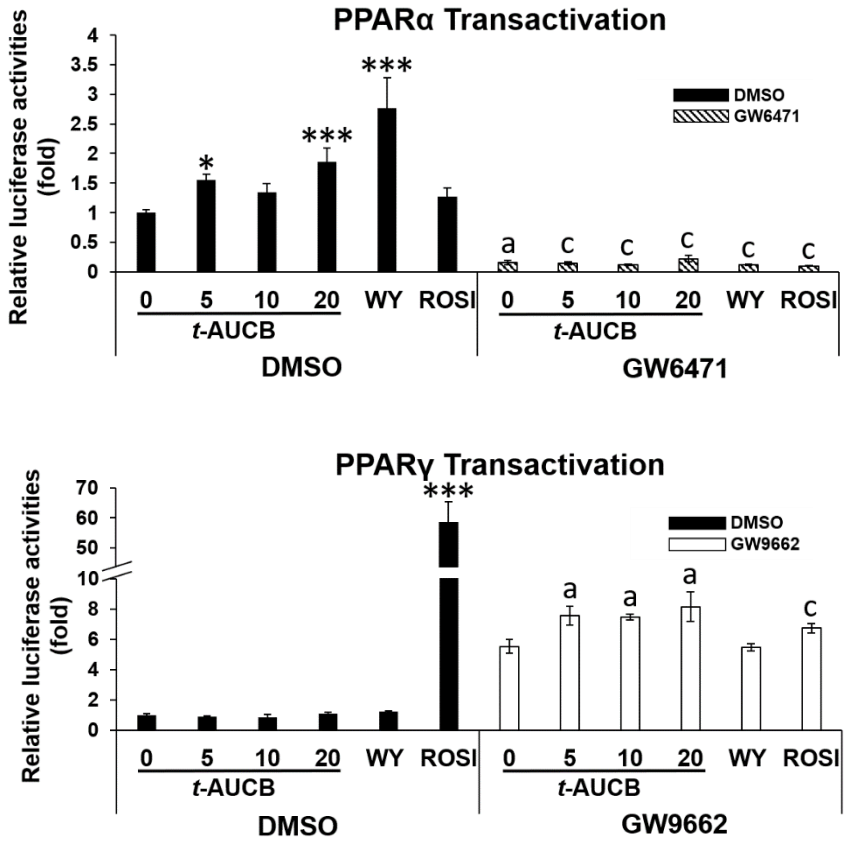

Figure 2. *t*-AUCB activates PPARα, but not PPARγ.

Murine brown preadipocytes were transiently transfected with murine (bottom panel) reporters. The transfected cells were pretreated with DMSO (control), PPARα antagonist GW6471 (10 μM), or PPARγ antagonist GW9662 (30 μM) for one hour. The cells were then treated with DMSO, GW6471, or GW9662 and *t*-AUCB (0, 5, 10, 20 μM), PPARα agonist WY-14643 (10 μM), or PPARγ agonist rosiglitazone (1 μM) for 18 hr. Relative luciferase activities were expressed as fold of the control samples (0) of each treatment group (DMSO, GW6471, or GW9662). Data=Mean±SEM (n=3). *, **, ***, $p<0.05$, $p<0.01$, and $p<0.001$, respectively, as compared to the control (0) of each treatment group (DMSO, GW6471, or GW9662). a, b, c, $p<0.05$, $p<0.01$, and $p<0.001$, respectively, for each treatment within GW6471 or GW9662 treatment groups as compared to its identical treatment within the DMSO treatment groups.

Figure 3. *t*-AUCB-induced upregulation of mRNA markers of thermogenesis and differentiation is attenuated by PPARα antagonist GW6471.

Upon initiation of differentiation, murine brown preadipocytes were pretreated with DMSO (control), PPARα antagonist GW6471 (10 μM), or PPARγ antagonist GW9662 (30 μM) for one hour then differentiated in the presence of DMSO, GW6471, or GW9662 and *t*-AUCB (0, 5, 10, 20 μM), PPARα agonist WY-14643 (10 μM), or PPARγ agonist rosiglitazone (1 μM) for 6 days. Total RNA samples were isolated on day 6. mRNA expression of brown marker genes *Pgc-1a*, *Pparg*, and *Ucp1* and general differentiation marker *Fabp4* are shown. Data=Mean±SEM (n=3). *,**, ***, $p<0.05$, $p<0.01$, and $p<0.001$, respectively, as compared to the control samples (0) of each treatment group (DMSO, GW6471, or GW9662). a, b, c, $p<0.05$, $p<0.01$, and $p<0.001$, respectively, for each treatment within GW6471 or GW9662 treatment groups as compared to its identical treatment within the DMSO treatment group.

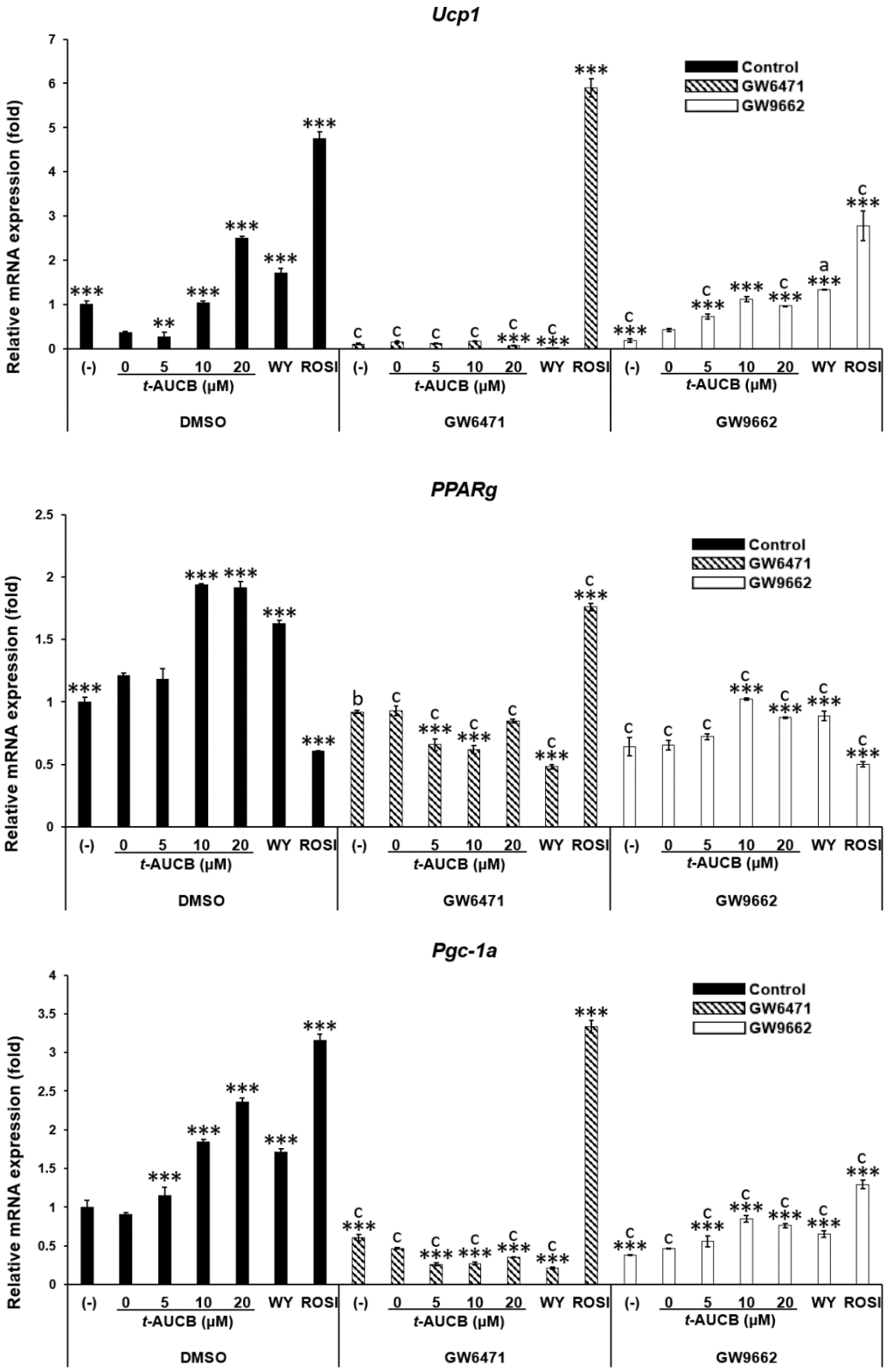

Figure 3 Continued

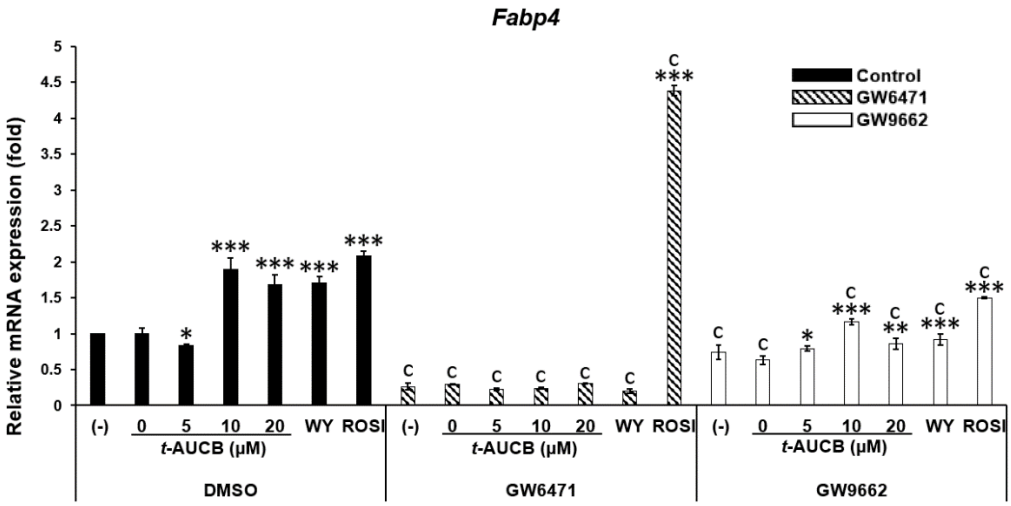

Figure 3 Continued

Figure 4. *t*-AUCB-induced upregulation of mRNA and protein markers of thermogenesis and differentiation is attenuated by PPARα knockdown.

Murine brown preadipocytes were infected with a scramble (control), PPARα KD, or PPARγ KD lentivirus containing a puromycin resistance gene. The cells were then subjected to puromycin selection for 2 weeks. Isolated clone and pool samples were collected for protein analysis. Selected clones were differentiated in the presence of *t*-AUCB (0, 10, 20 μM), PPARα agonist WY-14643 (10 μM), or PPARγ agonist rosiglitazone (1 μM) for 6 days. Total RNA and protein were isolated on day 6. (A) Protein expression of PPARα, PPARγ, and β-Actin (loading control) of selected control, PPARα KD, and PPARγ KD clones. Bar graphs show normalized densitometry for PPARα/β-Actin and PPARγ/β-Actin. (B) mRNA expression of brown marker genes *Ucp1*, *PGC-1a*, and *Cidea* and general differentiation marker *Fabp4* are shown. (C) Protein expression of UCP1, PGC-1α, FABP4, and ERK 1/2 (loading control) are shown. Bar graphs show normalized densitometry for UCP1/ERK 1/2, PGC-1α/ERK 1/2, and FABP4/ERK 1/2. Data=Mean±SEM (n=3). *,**, ***, $p<0.05$, $p<0.01$, and $p<0.001$, respectively, as compared to the control samples (0) of each group (control, PPARα KD, or PPARγ KD). a, b, c, $p<0.05$, $p<0.01$, and $p<0.001$, respectively, for each treatment within PPARα KD or PPARγ KD groups as compared to its identical treatment within the control group.

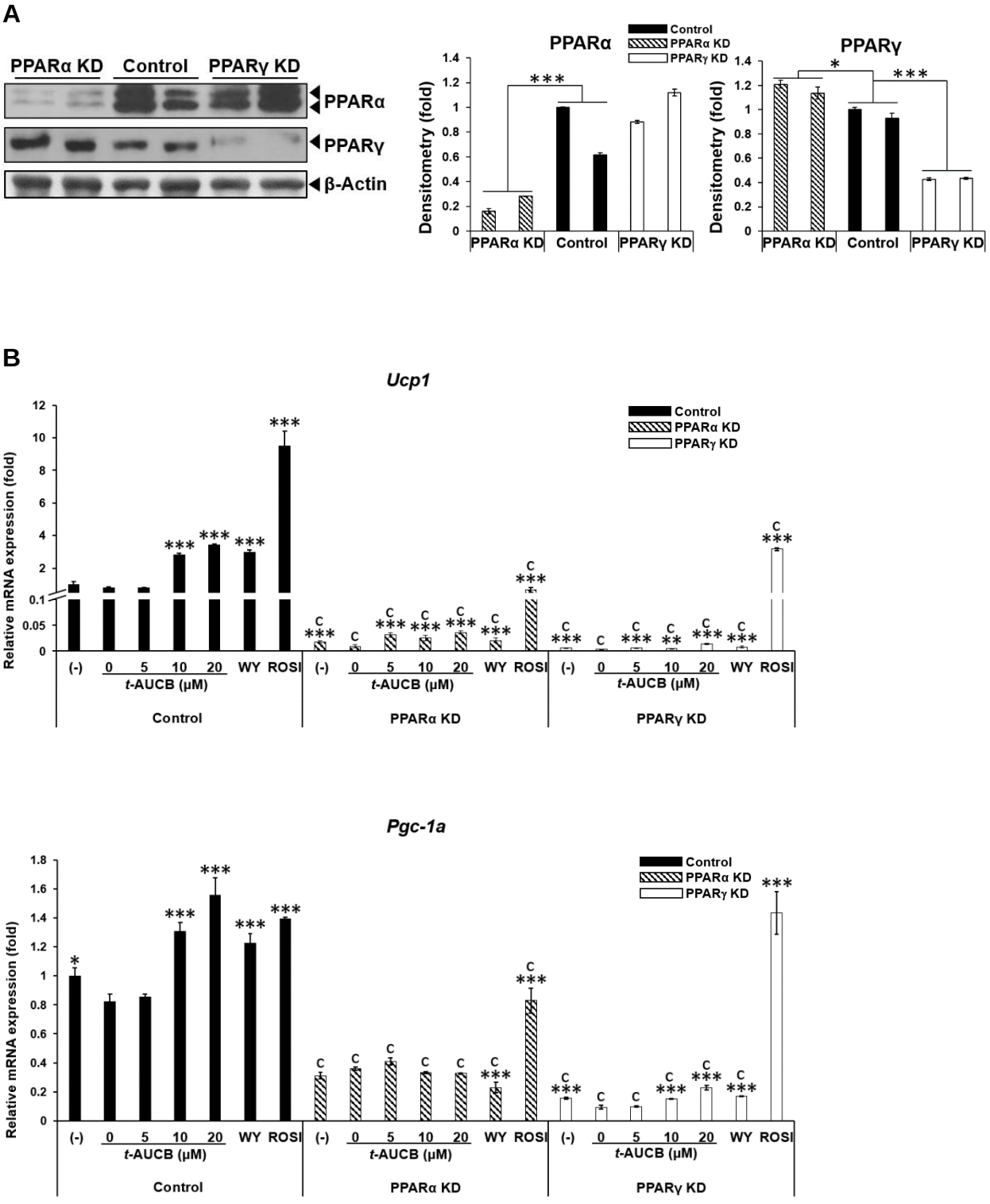

Figure 4 Continued

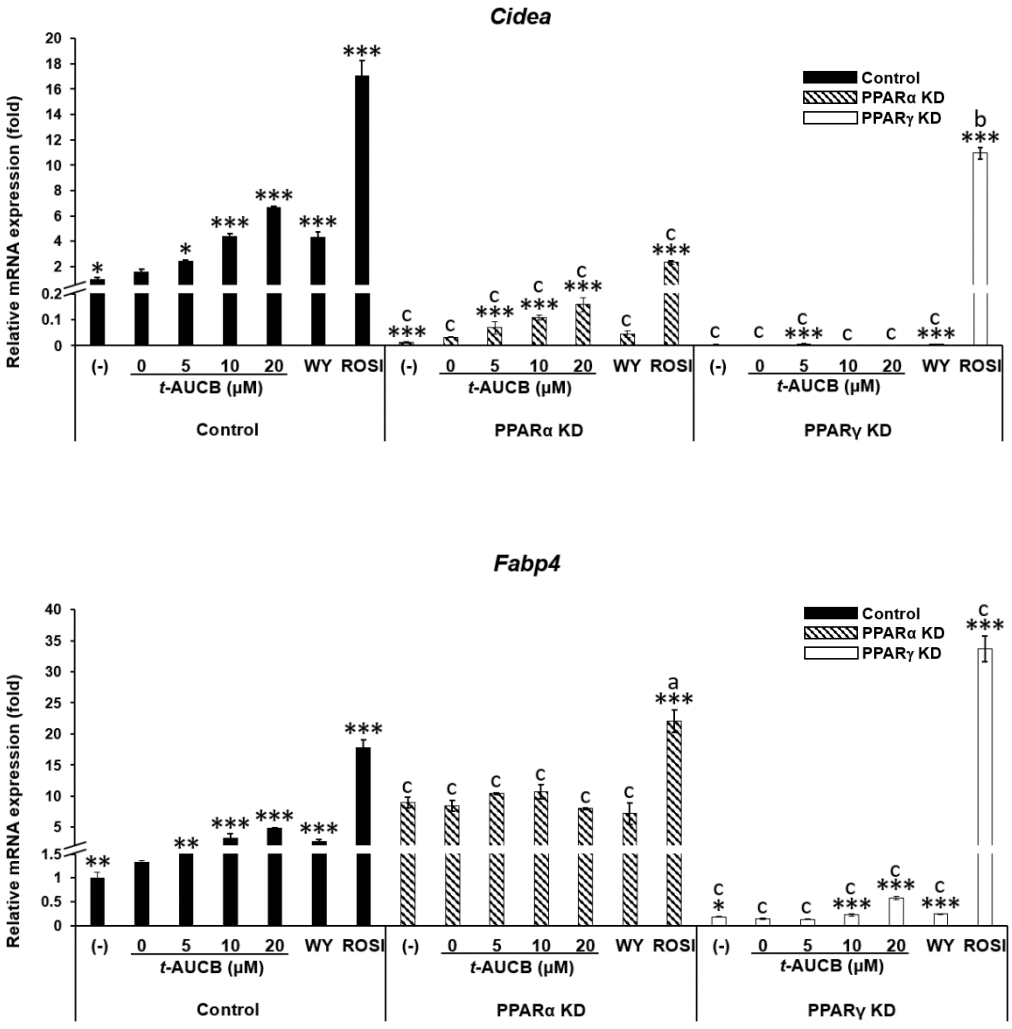

C

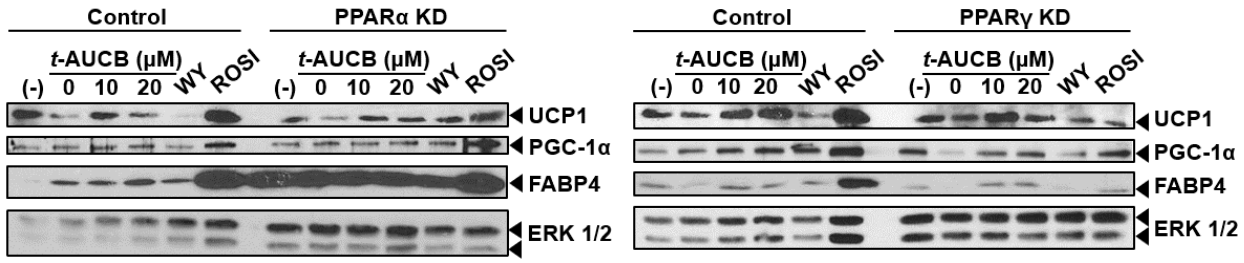

Figure 4 Continued

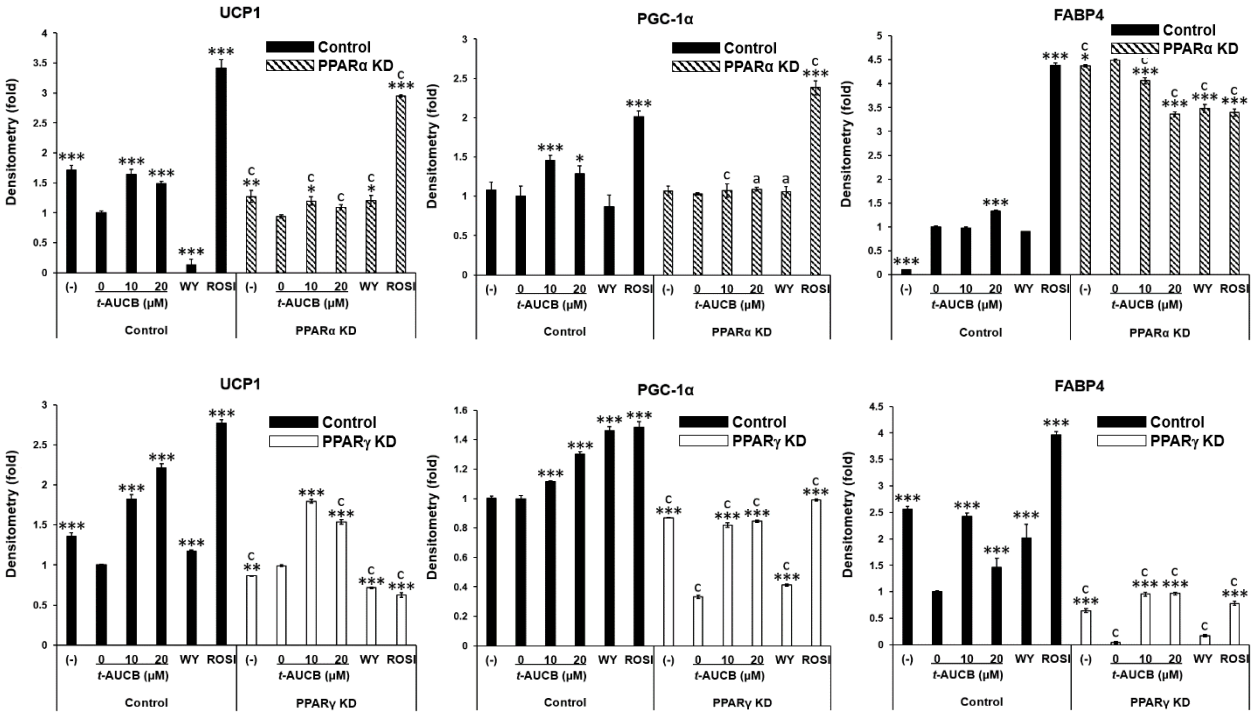

Figure 4 Continued

Figure 5. *t*-AUCB activates PPARα independent of sEH.

Murine sEH WT and sEH KO BAT stromal cells were differentiated for 7 days and protein samples were collected on day 0 and day 7. sEH WT and sEH KO BAT stromal cells were transiently transfected with murine PPARα or PPARγ reporters. The transfected cells were treated with *t*-AUCB (0, 10, 20 μM), PPARα agonist WY-14643 (20 μM), or PPARγ agonist rosiglitazone (1 μM) for 18 hr. (A) Protein expression of sEH and tubulin is shown. Bar graphs show normalized densitometry for Pparα/non-specific band and Pparγ/non-specific band. (B) Relative luciferase activities are shown as fold of the control samples (0) of each genotype (sEH WT or sEH KO). Data=Mean±SEM (n=3). *, **, ***, $p<0.05$, $p<0.01$, and $p<0.001$, respectively. a, b, c, $p<0.05$, $p<0.01$, and $p<0.001$, respectively, for each treatment within the sEH KO genotype groups as compared to its identical treatment within the sEH WT group.

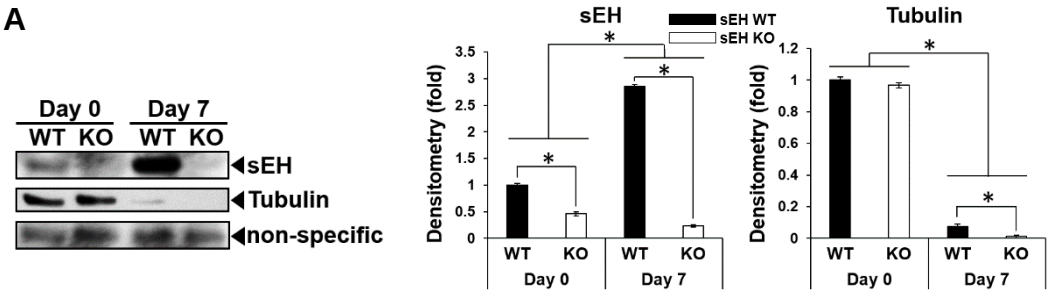

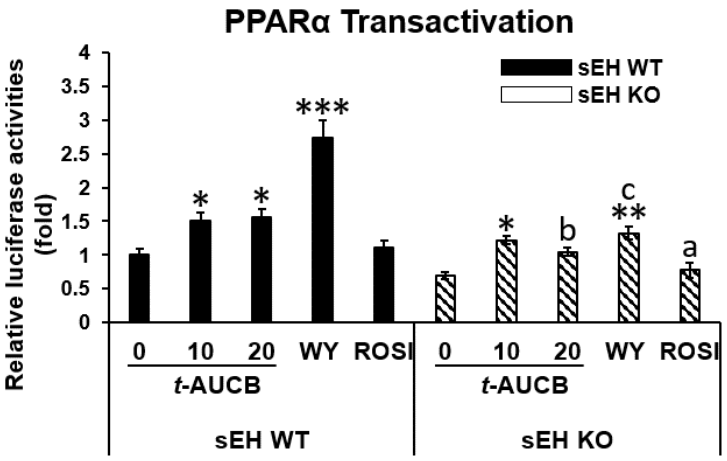

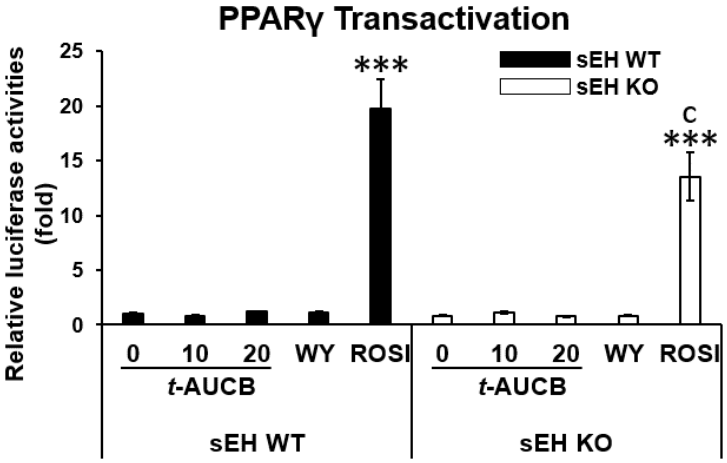

Figure 5 Continued

VITA

Kelsey Jo Hildreth was born to Michael and Beth Hildreth in Dodgeville, Wisconsin. She graduated from Byron High School in Byron, Illinois in 2014. In 2017 she completed her Bachelor of Science at Northern Illinois University, majoring in Nutrition, Health, and Wellness and minoring in Kinesiology and Biology. Upon graduation, she was accepted into the combined Master's/Dietetic Internship program with a concentration in Cellular and Molecular Nutrition at the University of Tennessee, Knoxville. During the program, she conducted her thesis research under Dr. Ling Zhao. During her time at UTK, she acted as a teaching assistant for Nutrition 313 and Nutrition 302. She completed her dietetic internship in August 2019. She defended her thesis on November 1st, 2019. Following graduation, Kelsey plans to sit for the Commission of Dietetic Registration exam.